Modeling, Analysis, and Verification of a Weld-Breaking Mechanism for Automatic Circuit Recloser Applications

Brian Korves
Marquette University

MODELING, ANALYSIS, AND VERIFICATION OF A WELD-BREAKING MECHANISM FOR AUTOMATIC CIRCUIT RECLOSER APPLICATIONS

by

Brian A. Korves, B.S.

A Thesis Submitted to the Faculty of the Graduate School,
Marquette University,
in Partial Fulfillment of the Requirements for
the Degree of Master of Science

Milwaukee, Wisconsin

August 2014

ABSTRACT

MODELING, ANALYSIS, AND VERIFICATION OF A WELD-BREAKING MECHANISM FOR AUTOMATIC CIRCUIT RECLOSER APPLICATIONS

Brian A. Korves, B.S.

Marquette University, 2014

The automatic circuit recloser (ACR) is responsible for protecting electrical distribution grids in the event that high voltage power lines come in contact with ground. In order to prevent damage, ACRs break the electrical continuity of the circuit through the use of a vacuum interrupter and a weld breaking mechanism. Vacuum interrupters consist of two metallic contacts in an air-tight ceramic housing. Due to the electrical interactions that take place during the interruption process, unintended welds are formed between the contacts. These welds have the ability to impede or completely stop the interruption process, thus rendering the ACR inoperable.

In order to ensure that the ACR can interrupt current even when welds have formed, a mechanism is used to complement the opening force and impart an impact load on the weld. This mechanism is generally designed based on rules of thumb and engineering judgement. This thesis develops a dynamic model of an ACR, which acts as a blueprint for the further development and optimization of the weld-breaking motion. The dynamic model consists of four main submodels: the dynamic motion of the masses, the dielectric breakdown model, the contact bounce model, and the weld-strength model. The dynamic motion and the weld-strength model are developed based on first principles, while the dielectric breakdown model and the contact bounce model are determined based on experimental data. The overarching dynamic model is compared to performance data and shows good agreement.

ACKNOWLEDGEMENTS

Brian A. Korves, B.S.

I would like to thank Dr. Philip Voglewede for the unbelievable amount of time and effort he put into advising me during this work and my entire academic career. Additionally, I would like to thank Dr. Mark Nagurka and Dr. Kevin Craig for their astute advice and suggestions. A special thanks goes to out to my fellow WedeLab members for their constant support and helpful advice. Finally, I would like to thank my family and friends for their lifelong love and encouragement.

DEDICATION

I would like to dedicate this work to my family. Without their continuous support throughout my life, I would not have had the strength to complete this thesis.

Thank You

TABLE OF CONTENTS

TABLE OF CONTENTS — *Continued*

TABLE OF CONTENTS — *Continued*

LIST OF FIGURES

LIST OF FIGURES — *Continued*

CHAPTER 1

Introduction

Many buildings are protected by circuit breakers that open in response to surges in the building's electrical system. In the event that a breaker is triggered, a person must manually seek out and reset the breaker. While this process takes place, no electricity is available for the devices within the building. The process of finding the breaker box and resetting the switch can occur quickly in the close confines of a single building. However, when dealing with the electrical grid for a much larger system, manual resetting of circuit breakers becomes a much more time-intensive process, as a technician would have to drive a potentially significant distance from the utility's station to the source of the interruption. The manual resetting process can result in significant outage times for the areas protected by the circuit breaker. These times can be excessively long in instances of extreme weather where multiple breakers can be triggered in a short time, with too few technicians to perform the resets in a timely manner. To make the situation more vexing, many of the breaker-triggering events clear themselves, meaning that normal operation could be restored after a few seconds, but are limited by the absence of a technician.

In order to address the increasing size of the electrical distribution grid and the desire for better customer service, a new kind of circuit breaker was designed. This new circuit breaker operated like a conventional breaker in that it had the ability to break the circuit when a fault current was detected. However, rather than remaining open, this circuit breaker has the ability to close the circuit again after a short pause in order to check if the fault had cleared. If the fault was present, this open/close process could continue for a predetermined number of operations. If the fault is still present after those additional operations, it would lock open and a signal would be sent to the utility. A line technician would then be required to find the source of the fault and clear it before manually resetting the circuit breaker. However, in most cases, the fault (such as a squirrel reaching from a power line to a grounded object) would have cleared itself within the allotted number of open/close operations, meaning that normal operation could be restored to the line immediately. Thus, the outage time was shortened from hours to seconds. This new style of circuit breaker was appropriately dubbed an automatic circuit recloser (ACR).

Automatic circuit reclosers are now commonly found in the electrical distribution grid. There are four main components of an ACR: vacuum interrupter (VI), weld-breaking mechanism, magnetic actuator, and epoxy encapsulation. The modeling of the vacuum interrupter and weld-breaking mechanism is the main focus of this research and they will be described further in the following paragraphs. However, before moving on to the mechanical modeling of the system, some of the electrical interactions must be reviewed in order to make future the discussion more understandable. Many of these effects influence the final design of these vacuum interrupters, as will be discussed in Chapter 2. Figure 1.1 provides a road map of the parts of the ACR and the electrical interactions and physical elements of modeling interest that will be discussed in the following sections.

1.1 Electrical Interactions

During opening and closing operations, there are several electrical interactions that become significant because of the high voltage and high current values. The most important of these is the breakdown of the dielectric, which is commonly called arcing. The arcing that occurs during an operation is the cause of the strong welds, which necessitate the weld-breaking mechanism that is being modeled in this research. Additionally, forces that become noticeable because of the high current values include the blow-off forces and the attractive magnetic force. These four topics will be discussed in greater detail in the following sections.

1.1.1 Dielectric Breakdown

The contacts used in ACRs (as with all matter) are made up of a framework of atoms. If the energy level of these atoms are great enough, one or multiple atoms can be removed from the framework. However, even before any atoms are removed from this framework, there are also electrons and other particles in the space

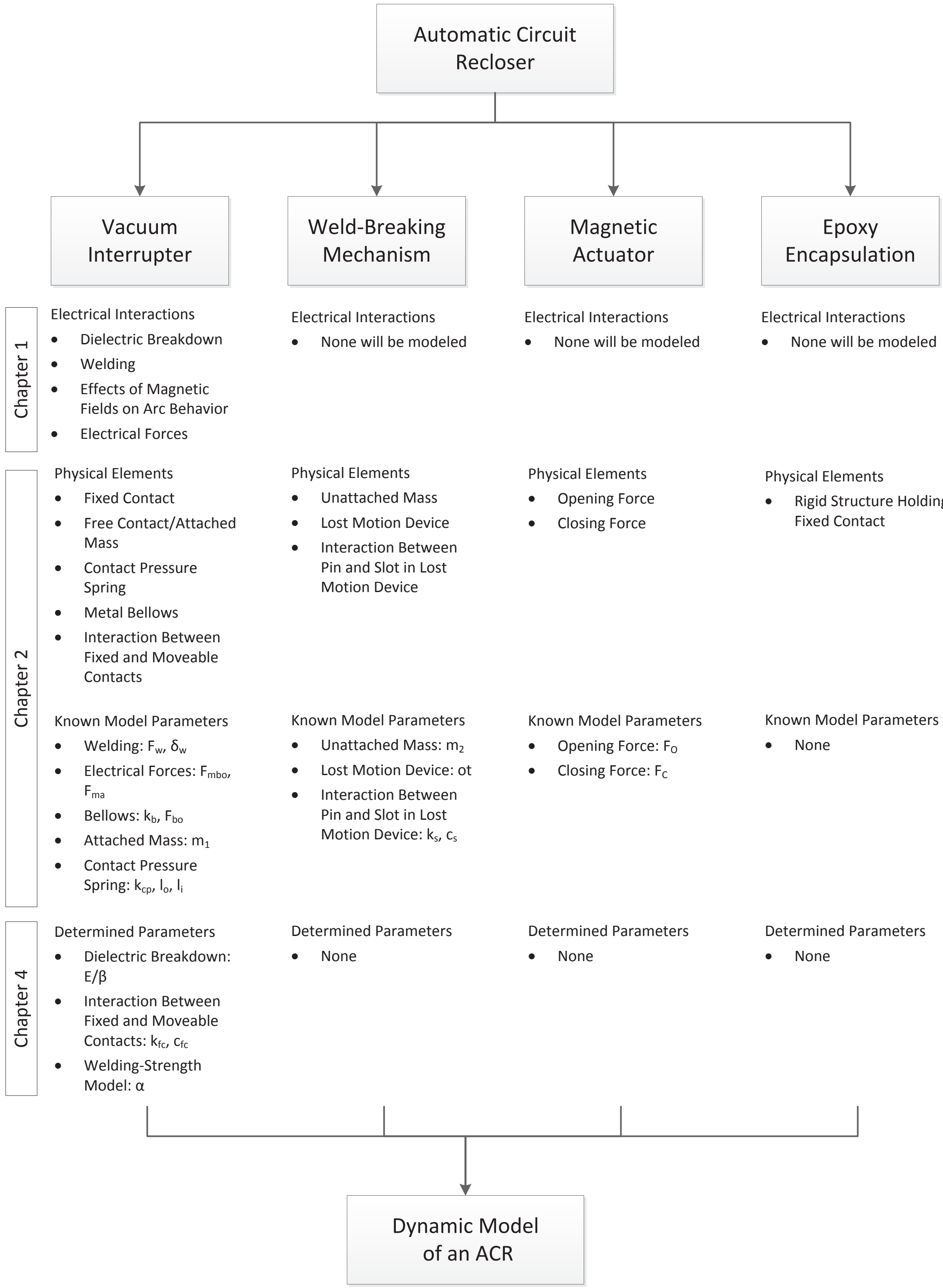

Figure 1.1: A road map of an ACR's components and electrical interactions.

between the contacts. When the voltage is applied between the contacts, it results in an electric field that produces a force on these free particles. Accelerated by the electric field, these particles will eventually hit the framework of atoms making up the contact face. This process imparts energy to the framework atoms, possibly resulting in the release of an electron or an ionized atom from the framework. This newly freed particle is also acted on by the electric field, causing it to accelerate and impact the surface framework, thus possibly freeing another electron or ionized atom. When a sufficient number of particles have been freed from the contact surfaces, a flow of electrons and ionized particles can be established between the contacts. This established flow is called the arc.

The theory behind utilizing vacuum as a dielectric for interruption and maintenance of electrical integrity is the reduction of the number of electrons and other particles in the space between the contacts. After all, it is the acceleration and subsequent impact of these particles that starts the chain reaction release of electrons and ions from the contact surface that results in arcing. The degree to which these particles have been removed is measured by the level of vacuum. According to Slade [2], vacuum interrupters often operate in the 10^{-2}-10^{-4} Pa range, which is classified as high vacuum. For comparison, the atmospheric pressure on the Earth at sea level is 101 kPa.

The prediction of when breakdown occurs is based on when the electric field strength reaches a level high enough to cause significant release of electrons and ions from the contact. This concept results in a fairly easy calculation because the contact gap and voltage level are known. However, the electric field can be intensified depending on the surface roughness characteristics and geometric enhancements, such as seen at the corners of the contacts. With these concepts in mind, the following model is used for the theoretical characterization of these events:

$$E_C = \frac{\beta_m \beta_g U}{d} \tag{1.1}$$

where the E_C term represents the critical electric field at which breakdown occurs, the U term represents the instantaneous voltage, and the d term represents the distance between the contact faces. The β_m term represents the microscopic field enhancement due to the surface roughness of the contacts and the β_g term represents the geometric field enhancement factor due to the shape of the contact. For this research, the model is bottle specific and therefore the β_m and β_g values were assumed to be relatively constant. These two terms were combined into a single β term, yielding Eqn. 1.2.

$$E_C = \frac{\beta U}{d} \tag{1.2}$$

It is important to note that some references show the field enhancement factor β in the denominator. Care should be taken when addressing the changes in the β and its affect on the E_C term. The next section will discuss how this arcing affects the performance of ACRs.

1.1.2 Welding

When arcing occurs during the opening and closing process, a considerable amount of energy is imparted to the contacts. This heating causes localized melting of the contact faces, which form welds when they are brought into contact and allowed to cool. Kulas [3] has developed a strategy for determining the size of the weld and the resulting maximum force required to break it. The energy transmitted by the arc, W_a, is known to be a function of the arc voltage (the voltage difference across the contacts when arcing is occurring), u_a, and the current value, $I(t)$, over the length of time that arcing occurs, t_a, as shown in Eqn. 1.3.

$$W_a = \int_0^{t_a} u_a I(t) dt \tag{1.3}$$

It is known that the amount of energy that goes into melting the mass of contact material that becomes the final weld is given by Eqn. 1.4,

$$W_c = m[c_V(T_m - T_0) + c_L] \tag{1.4}$$

where m is the mass of the welded material, c_V is the specific heat of the contact material, T_m is the melting temperature of the contact material, T_0 is the initial temperature of the contact material, and c_L is the latent heat of fusion of the contact material.

Determining the size of the weld requires setting $W_a = W_c$ and includes a number of inherent assumptions:

- Arcing occurs sufficiently fast that there is no heat transfer into the rest of the contact by conduction
- No heat transfer occurs by radiation into the interrupter atmosphere
- No arc energy is used to vaporize contact material

With these assumptions, it becomes possible to predict the mass of the weld based on the amount of energy absorbed by the contact during the closing process as a result of the dielectric breakdown.

Another part of the Kulas' work [3] was the development of a model for the max weld force. The maximum theoretical force, F_w, to break the weld as a function of W_c for pure copper contacts was found to be

$$F_W = 127W_c^{2/3} \tag{1.5}$$

This equation provides a theoretical limit for the weld force, which was then compared to experimentally measured values. Kulas [3] notes that the actual weld force was frequently below that calculated using Eqn. 1.5. The reasons for this include

- The arcing time was long enough that heat was able to conduct through the contact
- Arc energy was dissipated into the interrupter atmosphere
- The contact area locations varied during bouncing
- The motion of the arc roots, preventing the melting of a single weld nugget

Regardless, designing for these values provides assurance that the mechanism will be able to break strong welds. The weld model used in this research will be discussed in greater detail in Section 2.4. The focus of this research will be on dynamic welding, that is, the welding that occurs during the closing process. There is also a phenomenon called static welding, where the contacts weld together after prolonged contact. This static welding can be read about in [4] and [5]. Additionally, [6] utilizes a thermodynamical approach to discuss the diffusion of heat through the contact. This reference would be of particular interest should the assumption that no heat diffuses through the contact be relaxed.

1.1.3 Effects of Magnetic Fields on Arc Behavior

The arc that develops between two contacts can be heavily affected by the magnetic field that is present. If there is no modification made to the magnetic field that is present when current passes through a pair of linear conductors, the arc tends to progress from a diffuse arc or molten bridge into a full blown columnar arc. This arc is often constricted to a small fraction of the radius of the conductor and tends to remain stationary. However, the arc behaves much differently when within a transverse and axial magnetic field.

According to Slade [2], a columnar arc between two current carrying conductors will experience a force when in the presence of a magnetic field in a direction perpendicular to the current and arc length vectors, called a transverse magnetic field. The resulting force moves the arc across the face of the conductor, preventing it from remaining in a single location. This transverse magnetic field (TMF) can be caused by changing the shape of the conductors so that the current flows clockwise through one conductor and counterclockwise through the other (or vice versa).

The arc also behaves differently in an axial magnetic field (AMF). An arc exposed to an axial magnetic field will be converted from a columnar arc to a diffuse arc. This diffuse state means that the arc takes up the entire face area of the conductors and ensures that the entire face of the conductor receives the same amount of energy from the arc, meaning that no small area receives a disproportionately large share (as with a columnar arc). An axial magnetic field can be created in a pair on linear conductors by changing their shape so that the current flow is in the same direction when passing from one conductor to the next (i.e., clockwise/clockwise or counterclockwise/counterclockwise).

These effects are well known to VI designers and have been incorporated into many designs. The magnetic field can also affect the electrical forces that are seen in opening and closing operations, as will be discussed in the next section.

1.1.4 Electrical Forces

There are two forces due to the flow of electrons that are seen frequently in current carrying conductors. The first is due to the constriction of current from a large flow area to a smaller one (as seen in hydraulics when a fluid flows from a large diameter pipe to a pipe with a smaller diameter). This force is commonly referred to as the blow-off force, F_bo, and attempts to separate two touching conductors when current is flowing between them [7]. Its magnitude is given by Eqn. 1.6.

$$F_{bo} = 10^{-7} I(t)^2 \ln\left(\frac{R}{r}\right) \tag{1.6}$$

where $I(t)$ is the instantaneous current (Amps), R is the radius (meters) of the contact face, and r is the radius (meters) of the constriction area. The constriction area is the area of actual contact between the two contact faces. Due to the roughness of the contacts, the ratio of the contact radius to the constriction radius is generally considerably greater than 1. A general strategy is to use the hardness of the contact material H and the contact pressure force P to determine the constriction area A, as shown in Eqn. 1.7.

$$A = \pi r^2 = \frac{P}{H} \tag{1.7}$$

Regardless of contact choice, the blow-off force is substantial when the contacts are touching. However, AMF contacts create a diffuse arc that is the same radius as the contact face, the natural log term is zero and the blow-off force does not act. This effect prevents the blow-off forces seen during arcing with unmodified and TMF contacts.

The other electrical force is an attractive electro-magnetic force, $F_m a$ due to the parallel current flows used in AMF contacts. This force is based on Ampere's force law:

$$F = 2k_A \frac{I_1 I_2}{r} \tag{1.8}$$

where k_A is the magnetic force constant, r is the spacing between the wires, and the

I's are the current values. This force is also current dependent and is frequently designed into conductors in order to balance the blow-off force.

This section reviewed many of the electrical and mechanical interactions encountered in automatic circuit reclosers. The knowledge of many of these effects was utilized in the design of the ACR to be modeled and must be understood in order to create a valid model, as discussed in the following chapter.

CHAPTER 2

Modeling

When creating a dynamic model, the first step is to identify the physical system and the major factors and forces that will be considered. Once this has been done, the physical system is simplified to a physical model, which contains only the system characteristics that are required for a sufficient level of fidelity. The laws of nature are then applied to the physical model to create the mathematical model. It is this mathematical model that is simulated in order to predict the performance of the physical system. Each of the systems and models will be discussed in detail, starting with the physical system.

2.1 Physical System

The physical system being modeled in this research is made up of the ACR's main components:

- Vacuum Interrupter
- Weld-Breaking Mechanism
- Magnetic Actuator
- Epoxy Encapsulation

The epoxy encapsulation and magnetic actuator will be discussed only briefly, as they provide only fringe effects on the system. However, the vacuum interrupter and weld-breaking mechanism systems have a major impact on the performance of the ACR and will be discussed heavily in the following sections.

2.1.1 Vacuum Interrupter

In industrial electrical switching, several dielectric mediums have been used, with varying degrees of usefulness. The most popular were air, oil, SF6 gas, and

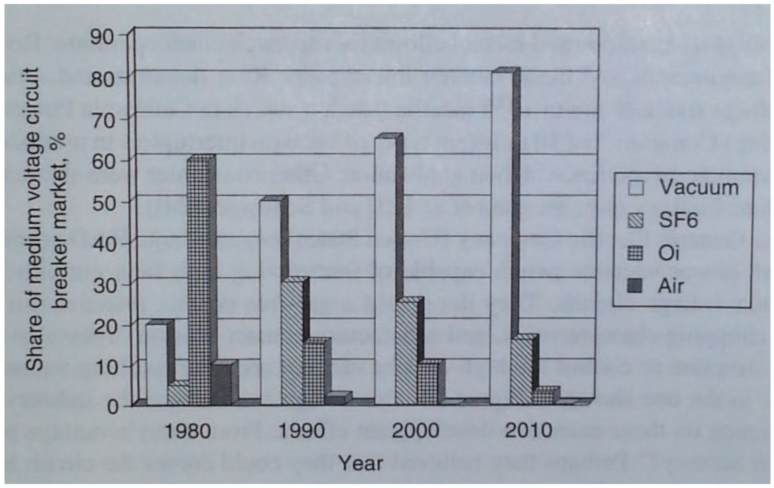

Figure 2.1: Plot showing the evolution of the usage of each main interruption medium over time. [2] Courtesy of CRC Press.

vacuum. As seen in Fig. 2.1, oil was the preferred dielectric in circuit breakers as recently as 1980. However, there is a clear trend of increasing vacuum dielectric use. SF6 gas spiked momentarily in 1990, but has since diminished. The use of oil and air has since dwindled to nearly nothing. The use of vacuum as a dielectric has clearly taken over the market.

While each manufacturer creates vacuum interrupters with slight variations, there are several key characteristics that are found in nearly all VI's and are called out in Fig. 2.2. VI's contain a pair of contacts that must be contained in a vacuum, so an insulating housing and metal bellows is utilized. These components will all be discussed in more detail in the following paragraphs. Finally, various shields are used to protect the bellows and housing from the high energy electrical interactions that occur during operation. The shields are accounted for in this model only for the mass they contribute to the moving contact; otherwise, they are ignored.

Contacts

Vacuum interrupters are composed of two metallic conductors encased in an airtight cylindrical ceramic housing. One of these conductors is fixed within the housing and is aptly called the fixed contact. The other contact is capable of axial linear motion relative to the housing and is referred to as the moveable contact. When these two conductors are touching, electrical continuity is achieved and current can flow through the ACR. It is the separation of the conductors that is the

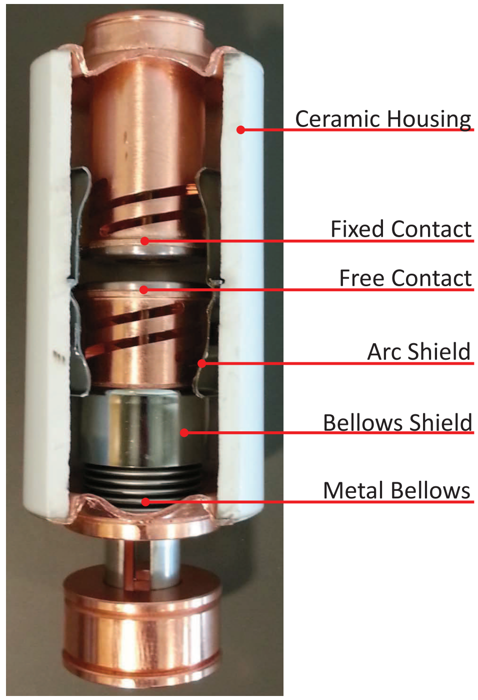

Figure 2.2: Diagram of a vacuum interrupter with the key components labeled.

main goal of an opening operation and the quickest possible mating of these conductors that is the main goal of a closing operation.

As discussed in Section 1.1.3, the presence of a magnetic field can affect the behavior of the arc that forms due to the small contact gaps during opening and closing operations. The vacuum interrupters under investigation in this research utilize an axial magnetic field (AMF) contact structure. This AMF is produced by cutting helical slots into the contact stem, as shown in Fig. 2.2. These helical slots force the current to flow in a spiral motion when it passes through the contact stem. These helical slots are present in both the fixed and moveable contacts and are responsible for the exclusive presence of a diffuse arc and the attractive magnetic forces due to the parallel current flows.

The vacuum interrupters examined in this thesis utilize two different contact materials. Some bottles use contact material that is a mixture of 65% Chromium and 35% Copper, while others use a mixture of 30% Chromium and 70% Copper. These changes have relatively little affect on the proposed dynamic model, but do require a change in the coefficients used in the function used for the determination of the arc voltage. However, this change in contact material does not affect the weld strength model, as nominal values for copper are currently used exclusively, as was discussed earlier in the welding section of the introduction and will be discussed further in the physical model section.

Contact Pressure Spring

One of the key components of a vacuum interrupter is the contact pressure spring. During the initial operation of the finely processed contacts, it is known that some contact compaction is seen due to the plastic deformation of the contacts due to the high loads seen at impact. When high fault currents are flowing through the contacts, it is important to maintain a significant area of actual contact between the contact surfaces. If this area becomes small, the blow-off forces become significant and the resistance between the contacts increases, leading to localized melting. A spring, called the contact pressure spring is used to provide a compliant force between the contacts that can account for the contact compaction. It is the energy stored in this contact pressure spring during the closing operation that is responsible for the majority of the energy used to break the weld during an opening operation.

Bellows

A metal bellows is used to allow the moveable contact to move relative to the ceramic housing without breaking the vacuum seal. These metal bellows are made of 300 series stainless steel, giving them the ability to withstand the volatile environment that occurs during operation. They are quite robust when expanded and contracted in the axial direction, but are very intolerant of any twisting motion. For this reason, special anti-twist provisions have been made to ensure that the moveable contact only translates.

2.1.2 Weld Breaking Mechanism

The mechanism responsible for breaking the welds formed between the contacts is constructed to provide an impact load on the free contact. Its operation involves the acceleration of a large mass over some distance (called the overtravel) before the large mass (called the unattached mass) hits the free contact (called the attached mass) through a lost motion mechanism. The contact pressure spring along with a force supplied by a magnetic actuator is responsible for accelerating the unattached mass. As mentioned earlier, the contact pressure spring is also used to counteract blow-off forces and maintain substantial contact between the fixed and moveable contacts during spikes of fault current. The preload on the spring and the amount of overtravel are balanced to ensure that enough energy is available to break the weld and to ensure that the proper forces are maintained between the contacts after contact compaction has occurred.

2.1.3 Magnetic Actuator

The magnetic actuator is responsible for the opening and closing forces that act on the unattached mass. This actuator is composed of a large solenoid coil that produces appropriate forces based on the controlled current that is run through it. The electrodynamics of this system are assumed to be fast compared to the dynamics of the opening and closing operations. Therefore, this system is modeled as step change. The closing force is also modeled as instantaneous, but is known to decrease. This decrease in force is implemented to reduce the energy that must be absorbed by the structure when the unattached mass reaches the end of its stroke. Therefore, it will be modeled as a decreasing ramp, starting at some maximum value and ending at zero over the stroke of the mechanism.

2.1.4 Epoxy Encapsulation

The vacuum interrupter is encased within an epoxy encapsulation (the origin of the name *ecap* or *encap* used when referring to ACRs). This encapsulation is a rigid housing that provides protection for the interrupter and a dielectric matrix for the assembly of the additional shields and current carrying terminals, as well as the means of attaching the ACR to the tank that contains the actuator. Also, the exterior of the encapsulation also furnishes the ACR with the sheds that are required to provide the appropriate creep distance between the high- and low-voltage terminals. The epoxy encapsulation is only included in the model as a means of specifying the fixed terminal and ceramic housing of the vacuum interrupter as fixed to ground.

Now that the main components of the physical system have been established,

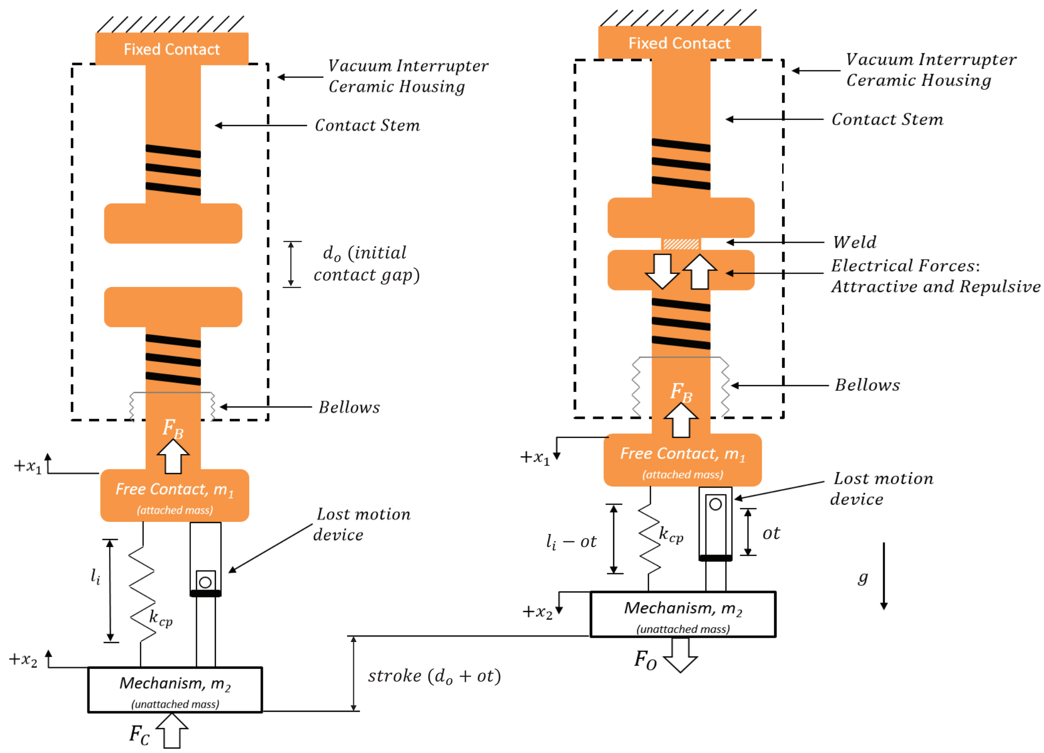

Figure 2.3: Physical models for the closing (left) and opening (right) processes.

the physical model will now be described.

2.2 Physical Model

The key difference between the physical system and physical model are the simplifying assumptions applied to each component of the physical system. Table 2.1 shows each component of the physical system, how it is modeled, and the assumptions inherent in that model. Each of the components shown in the table are shown graphically in Fig. 2.3.

While many of these models and assumptions are very straightforward, the contact models are worthy of additional discussion. Contact must be modeled at three locations: between the fixed contact and the attached mass, between the pin and the bottom of the slot of the lost motion device, and between the pin and the top of the slot of the lost motion device. The Kelvin-Voight model of contact, shown in Fig. 2.4, utilizes a spring (k) and damper (b) in parallel [8]. This model is used to represent collisions where there is some energy storage and some energy loss.

Table 2.1: Models and Assumptions for Each Physical System Component

Physical System Component:	*Modeled As:*	*Assumptions:*
Attached Mass (Moveable Contact)	- point mass	- rigid body - anti-twist collar prevents rotation
Unattached Mass	- point mass	- rigid body - anti-twist collar prevents rotation
Fixed Contact	- rigid structure	- ecap is sufficiently rigid - interrupter housing does not deform
Contact between Fixed and Moveable Contacts	- standard Kelvin-Voight spring and damper pair (both pure and ideal)	- contact material is viscoelastic
Contact Pressure Spring (CPS)	- pure and ideal spring	- mass of CPS is negligible - obeys Hooke's Law
Bellows	- pure and ideal spring	- bellows mass is negligible - obeys Hooke's Law
Blow-Off Force	- step input	- zero rise time - acts when contacts are touching - follows Eqn. 1.6
Magnetic Attractive Force	- step input	- zero rise time - acts when current is flowing
Closing Force	- step input	- actuator electrical time constant is sufficiently fast
Opening Force	- value ramps down from maximum to zero	- actuator electrical time constant is sufficiently fast
Contact Between Pin and Slot Ends	- standard Kelvin-Voight spring and damper pair (both pure and ideal)	- pin and slot ends are viscoelastic

The spring represents the storage of the energy, as with elastic deformation. The damper represents the energy dissipation, as with plastic deformation, sound, heat, etc. As the bulk of this energy is given off during the initial strike and compression, the damper is active only when the attached mass is compressing the fixed contact. During the restitution phase, only the spring is active.

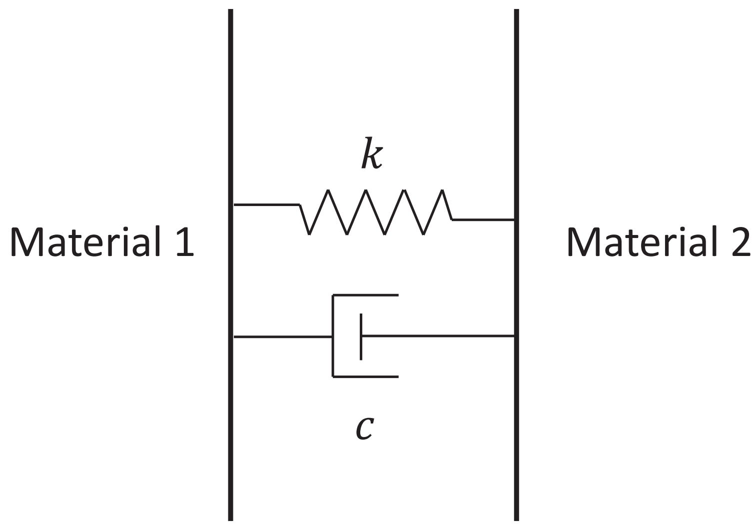

Figure 2.4: Graphical representation of Kelvin-Voight Model [8]

2.3 Mathematical Model

Once the simplifying assumptions had been applied to the physical system to create the physical model, the laws of nature were applied to the physical model to determine the mathematical model. The opening and closing motions have been divided into phases in order to account for the changes in the forces that are applied to the masses as they change position. The following section will outline the development of the mathematical model for a closing and opening operation.

2.3.1 Closing Operation

The four phases in the closing operation are as follows: approach phase, compression phase, terminal phase, and chatter phase (shown in Fig. 2.5). The sections below include a description of each phase, the corresponding free body diagrams, and the equations of motion for that phase. The nomenclature used in the free body diagrams is given in Table 2.2. The equations of motion for all phases

Table 2.2: Nomenclature used in the free body diagrams

Symbol	Physical Representation
F_C	Closing force due to the magnetic acutator
F_O	Opening force due to the magnetic acutator
F_{CPS}	Force due to the contact pressure spring
F_B	Force due to the bellows
F_{ks}	Force due to spring component of contact model between the pin and the mechanism slot
F_{cs}	Force due to damper component of contact model between the pin the the mechanism slot
F_g	Force due to gravity
F_{mbo}	Blow-off force
F_{ma}	Magnetic attractive force
F_w	Force due to the weld
$F_{electric}$	- Closing Operation: $F_{electric} = F_{ma} - F_{mbo}$ - Opening Operation: $F_{electric} = F_{mbo} - F_{ma} - F_w$
F_{kfc}	Force due to spring componenet of contact model between fixed contact and attached mass
F_{cfc}	Force due to damper component of contact model between fixed contact and unattached mass

of the closing operation are summarized in Table 2.3.

Approach Phase

The approach phase includes all times when the attached mass position is less than the initial gap between the contacts and the unattached mass position is less than the sum of the initial contact gap and the overtravel (meaning the contacts are not touching). This combination of the initial contact gap and overtravel is referred to as the mechanism stroke. During this phase, the closing force and bellows force are acting on the attached mass and the force transmits through the contact pressure spring to cause the unattached mass to accelerate. This phase is broken into two conditions. The first is when the attached mass has moved a greater distance than the unattached mass. A key interaction in this part of the

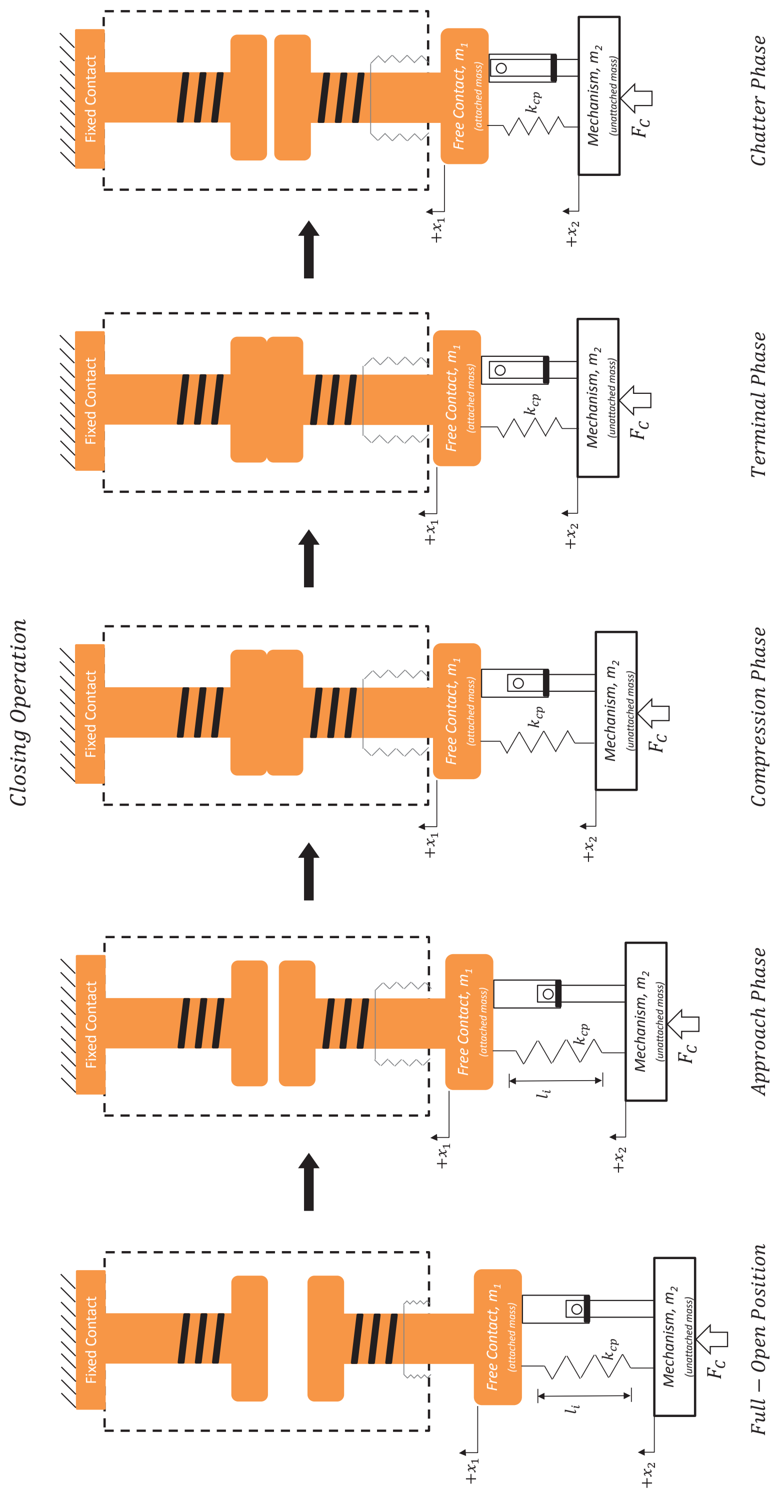

Figure 2.5: Approach, compression, terminal, and chatter phases that represent the contact motion during the closing operation.

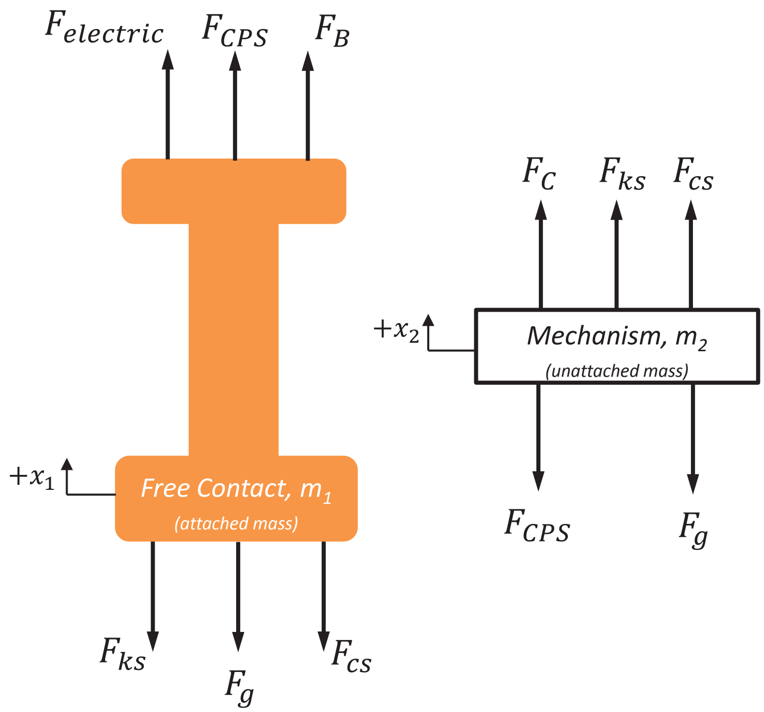

Figure 2.6: Free body diagrams for the approach phase while pin/slot contact is engaged

approach phase is the spring/damper (k_s, c_s) pair representing the contact forces between the pin and the end of the slot in the lost motion device. In terms of the overall mechanism, this contact is used to maintain the preload on the contact pressure spring. The free body diagram is shown in Fig. 2.6 and the resulting equation of motion are shown in Eqns. 2.1 and 2.2. The second part of this phase is when the unattached mass has traveled further than the attached mass. During this part of the approach phase, the spring/damper pair representing the contact between the pin and the end of the slot of the lost motion device is not active. The free body diagram for this condition is shown in Fig. 2.7 and the resulting equations of motion are shown in Eqns. 2.3 and 2.4.

$$\ddot{x}_1 = \frac{1}{m_1}[k_{cp}(l_o - l_i - x_1 + x_2) + F_{bo} + k_b(d_o - x_1) - m_1 g + F_{electric} + k_s(x_2 - x_1) + c_s(\dot{x}_2 - \dot{x}_1)] \quad (2.1)$$

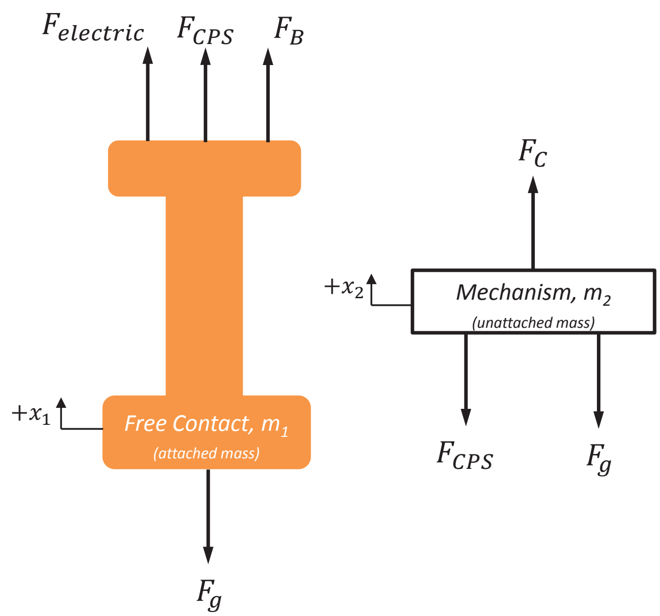

Figure 2.7: Free body diagrams for the approach phase after pin/slot contact ends

$$\ddot{x}_2 = \frac{1}{m_2}[F_c - k_{cp}(l_o - l_i - x_1 + x_2) - m_2 g - k_s(x_2 - x_1) - c_s(\dot{x}_2 - \dot{x}_1)] \tag{2.2}$$

$$\ddot{x}_1 = \frac{1}{m_1}[k_{cp}(l_o - l_i - x_1 + x_2) + F_{bo} + k_b(d_o - x_1) - m_1 g + F_{electric}] \tag{2.3}$$

$$\ddot{x}_2 = \frac{1}{m_2}[F_c - k_{cp}(l_o - l_i - x_1 + x_2) - m_2 g - k_s(x_2 - x_1) - c_s(\dot{x}_2 - \dot{x}_1)] \tag{2.4}$$

Compression Phase

The compression phase refers to situations in which the attached mass position is greater than or equal to the initial contact gap, but the unattached mass position is still less than the stroke (i.e., the contacts are touching). In this case the free contact is touching the fixed contact and the contact pressure spring is not yet at its full compression. A key change between the approach and compression phases is the addition of the spring/damper pair representing the contact forces between the attached mass and the fixed contact. The free body diagram is shown in Fig.

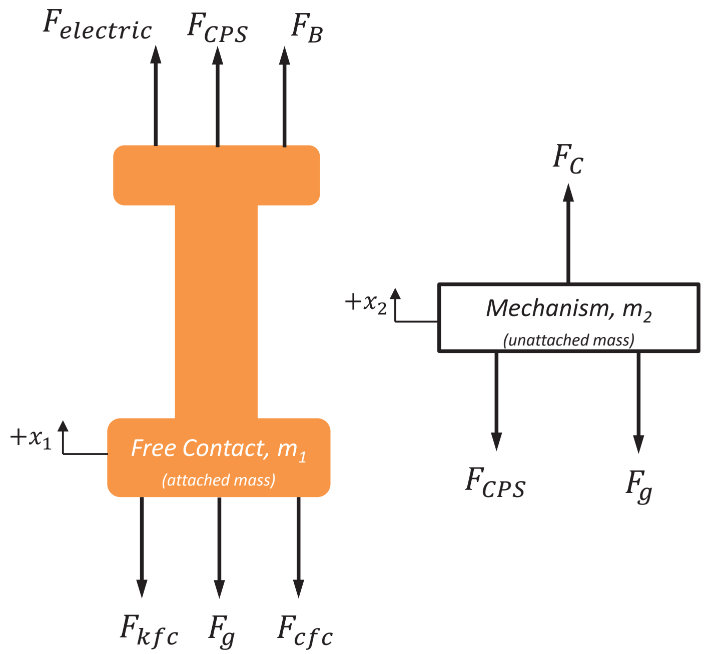

Figure 2.8: Free body diagrams for the compression phase

2.8 and the resulting equation of motion are shown in Eqn. 2.5 and 2.6.

$$\ddot{x}_1 = \frac{1}{m_1}[k_{cp}(l_o - l_i - x_1 + x_2) + F_{bo} + k_b(d_o - x_1) - m_1 g + F_{electric} \\ - k_{fc}(x_1 - d_o) - c_{fc}\,\dot{x}_1] \quad (2.5)$$

$$\ddot{x}_2 = \frac{1}{m_2}[F_c - k_{cp}(l_o - l_i - x_1 + x_2) - m_2 g] \quad (2.6)$$

Terminal Phase

The terminal phase describes the final resting position of the mechanism. In this phase the unattached mass position is greater than or equal to the initial contact gap and the attached mass position is greater than or equal to the stroke. The key change in the terminal phase is the addition of another spring/damper pair that creates the contact between the pin and the top of the slot in the lost motion device. Additionally, there is a latching mechanism that is activated when the unattached mass reaches the mechanism stroke length. For this reason, the

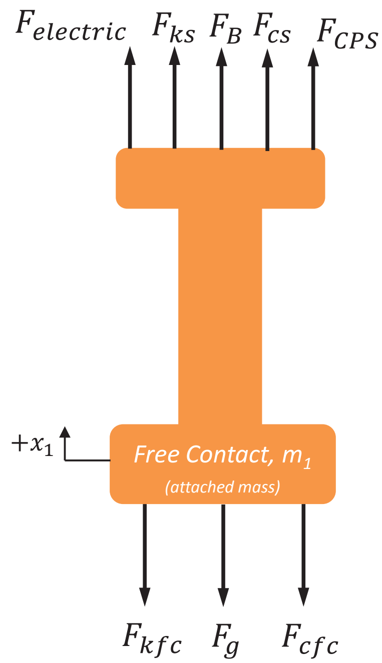

Figure 2.9: Free body diagram for the terminal phase

acceleration and velocity of the unattached mass is artificially brought to zero to ensure that the unattached mass does not move while the behavior of the attached mass is observed. The fixed contact is still in contact with the attached mass, so the spring/damper representing that contact is still required. The equation for this phase is shown in Eqn. 2.7.

$$\begin{aligned}\ddot{x}_1 = \tfrac{1}{m_1}[&k_{cp}(l_o - l_i - x_1 + x_2) + F_{bo} + k_b(d_o - x_1) - m_1 g + F_{electric} - k_{fc}(x_1 - d_o) \\ &- c_{fc}(\dot{x}_1) + k_{s2}(x_2 - ot - x_1) + c_{s2}(\dot{x}_2 - \dot{x}_1)]\end{aligned} \tag{2.7}$$

Chatter Phase

Sometimes during the transition from the compression phase to the terminal phase, bouncing occurs between the fixed contact and the moveable contact while the unattached mass is at a position greater than or equal to the mechanism travel. This situation would result in the attached mass being at a position less than the initial contact gap and the unattached mass being at a position greater than or equal to the mechanism stroke (where its acceleration and velocity are artificially held at zero). The key difference between the chatter phase and the terminal phase

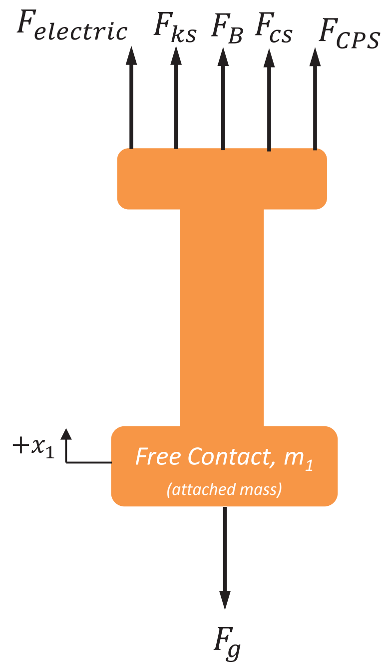

Figure 2.10: Free body diagram for the chatter phase

is that there is no contact between the fixed contact and the free contact, shown in Eqn. 2.8.

$$\ddot{x}_1 = \frac{1}{m_1}[k_{cp}(l_o - l_i - x_1 + x_2) + F_{bo} + k_b(d_o - x_1) - m_1 g + F_{electric} \\ + k_{s2}(x_2 - ot - x_1) + c_{s2}(\dot{x}_2 - \dot{x}_1)] \tag{2.8}$$

2.3.2 Opening Operation

The two phases in the opening operation are the extension phase and the retreat phase (shown in Fig. 2.11). The sections below include a description of each phase. The equations of motion for each phase can be found in Table 2.4. The motion of the attached and unattached masses after the contact gap has been restored is not of any interest, so the simulation is stopped once the retreat phase has finished. It should be noted from Fig. 2.3 that the datum and positive displacement directions are changed from the closing operation datum and positive displacement.

Table 2.3: Equations of Motion for All Phases of the Closing Operation

Approach Phase Before Initial Impact: $\ddot{x}_1 = \frac{1}{m_1}[k_{cp}(l_o - l_i - x_1 + x_2) + F_{bo} + k_b(d_o - x_1) - m_1 g + F_{electric} + k_s(x_2 - x_1) + c_s(\dot{x}_2 - \dot{x}_1)]$ $\ddot{x}_2 = \frac{1}{m_2}[F_c - k_{cp}(l_o - l_i - x_1 + x_2) - m_2 g - k_s(x_2 - x_1) - c_s(\dot{x}_2 - \dot{x}_1)]$ After Initial Impact: $\ddot{x}_1 = \frac{1}{m_1}[k_{cp}(l_o - l_i - x_1 + x_2) + F_{bo} + k_b(d_o - x_1) - m_1 g + F_{electric}]$ $\ddot{x}_2 = \frac{1}{m_2}[F_c - k_{cp}(l_o - l_i - x_1 + x_2) - m_2 g]$
Compression Phase $\ddot{x}_1 = \frac{1}{m_1}[k_{cp}(l_o - l_i - x_1 + x_2) + F_{bo} + k_b(d_o - x_1) - m_1 g + F_{electric} - k_{fc}(x_1 - d_o) - c_{fc}(\dot{x}_1)]$ $\ddot{x}_2 = \frac{1}{m_2}[F_c - k_{cp}(l_o - l_i - x_1 + x_2) - m_2 g]$
Terminal Phase $\ddot{x}_1 = \frac{1}{m_1}[k_{cp}(l_o - l_i - x_1 + x_2) + F_{bo} + k_b(d_o - x_1) - m_1 g + F_{electric} - k_{fc}(x_1 - d_o) - c_{fc} * \dot{x}_1 + k_{s2}(x_2 - ot - x_1) + c_{s2}(\dot{x}_2 - \dot{x}_1)]$
Chatter Phase $\ddot{x}_1 = \frac{1}{m_1}[k_{cp}(l_o - l_i - x_1 + x_2) + F_{bo} + k_b(d_o - x_1) - m_1 g + F_{electric} + k_{s2}(x_2 - ot - x_1) + c_{s2}(\dot{x}_2 - \dot{x}_1)]$

Extension Phase

The extension phase refers to the situations in which the unattached mass position is less than the mechanism overtravel. In this case, the attached mass is held between the contact pressure spring and the fixed contact. The contact pressure spring extends, accelerating the unattached mass away from the attached mass with the help of the opening force. Also, the weld force according to the curve determined by the previous closing operation is active. The free body diagram is shown in Fig. 2.12 and the resulting equations of motion are shown in Eqns. 2.9 and 2.10.

$$\ddot{x}_1 = \frac{1}{m_1}[-k_{cp}(l_o - l_i - ot - x_1 + x_2) - F_{bo} - k_b(x_1) + m_1 g + k_{fc}(-x_1) + c_{fc}(\dot{x}_1) + F_{electric}] \quad (2.9)$$

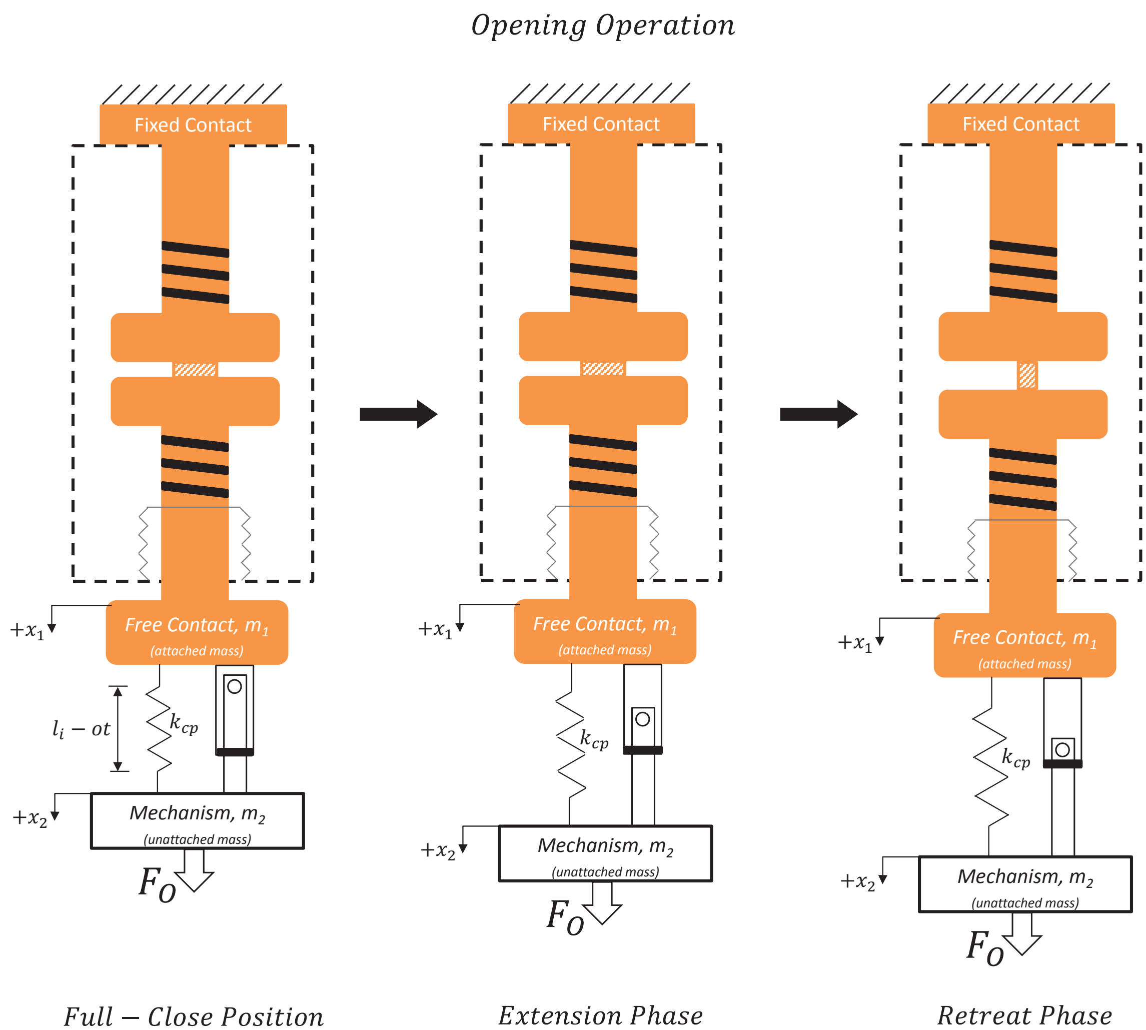

Figure 2.11: Extension and retreat phases that represent the contact motion during the opening operation.

$$\ddot{x}_2 = \frac{1}{m_2}[F_o + k_{cp}(l_o - l_i - x_1 + x_2) + m_2 g] \tag{2.10}$$

Retreat Phase

The retreat phase includes all times in which the unattached mass position is between the mechanism overtravel and the device stroke. The first key difference between the retreat phase and the extension phase is the addition of the spring/damper pair modeling the contact between the pin and the end of the slot. The second difference is the removal of the spring/damper pair modeling the contact between the attached mass and the fixed contact. The weld force is still

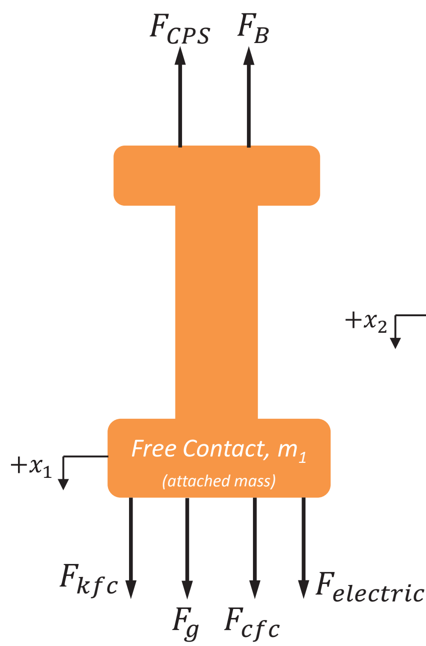

Figure 2.12: Free body diagrams for the extension phase

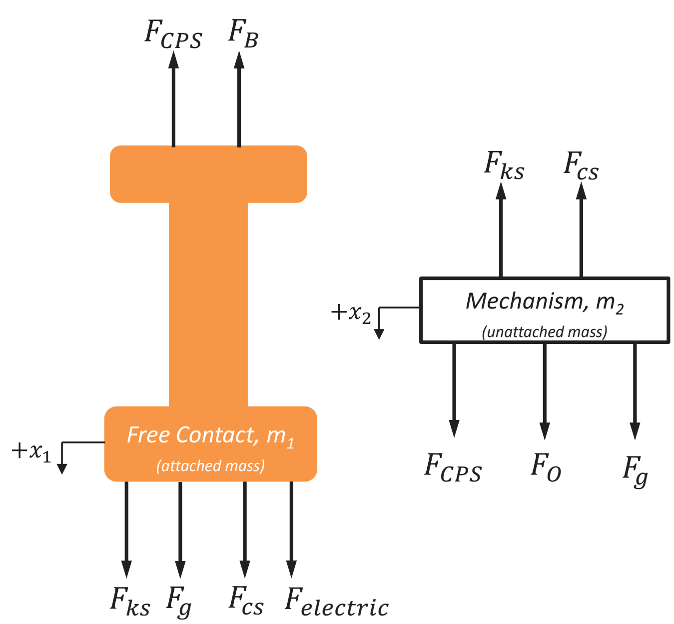

Figure 2.13: Free body diagrams for the retreat phase

active during this phase. The free body diagram is shown in Fig. 2.13 and the resulting equation of motion are shown in Eqns. 2.11 and 2.12.

Table 2.4: Equations of Motion for All Phases of the Opening Operation

Extension Phase
$\ddot{x}_1 = \frac{1}{m_1}[-k_{cp}(l_o - l_i - ot - x_1 + x_2) - F_{bo} - k_b(x_1) + m_1 g + k_{fc}(-x_1) + c_{fc}(\dot{x}_1) + F_{electric}]$
$\ddot{x}_2 = \frac{1}{m_2}[F_o + k_{cp}(l_o - l_i - x_1 + x_2) + m_2 g]$
Retreat Phase
$\ddot{x}_1 = \frac{1}{m_1}[-k_{cp}(l_o - l_i - ot - x_1 + x_2) - F_{bo} - k_b(x_1) + m_1 g + k_s(x_2 - ot - x_1) + c_s(\dot{x}_2 - \dot{x}_1) + F_{electric}]$
$\ddot{x}_2 = \frac{1}{m_2}[F_o + k_{cp}(l_o - l_i - x_1 + x_2) + m_2 g - k_s(x_2 - ot - x_1) - c_s(\dot{x}_2 - \dot{x}_1)]$

$$\ddot{x}_1 = \frac{1}{m_1}[-k_{cp}(l_o - l_i - ot - x_1 + x_2) - F_{bo} - k_b(x_1) + m_1 g + k_s(x_2 - ot - x_1) + c_s(\dot{x}_2 - \dot{x}_1) + F_{electric}] \tag{2.11}$$

$$\ddot{x}_2 = \frac{1}{m_2}[F_o + k_{cp}(l_o - l_i - x_1 + x_2) + m_2 g - k_s(x_2 - ot - x_1) - c_s(\dot{x}_2 - \dot{x}_1)] \tag{2.12}$$

2.4 Weld-Strength Model

The weld strength model utilizes the methods described in Section 1.1.2 to determine the size and maximum strength of the weld. This information is then used to determine the force of the weld as a function of the extension of the weld. Because the weld-breaking action is a high strain rate process, the shape of this curve is a topic of discussion. Dui [9] represents the forces required during a fracture as a linear decrease from some maximum initial force value to zero over some extension. However, the Dui model assumes that there is a crack of appreciable size in the material. One group of researchers found that the separation of contacts is roughly a 25%, 25%, 50% split between ductile failure, brittle failure, and some combination of ductile and brittle failure, respectively, when using copper contacts [10]. On the same topic, Greenwood presents curves corresponding to simplified ductile and brittle failure [11]. In a more general study, Johnson, et al. [1]

performed a series of experiments at impact (high) rates of strain. These high strain rate curves (see Fig. 2.14) look very much like the conventional low strain rate curves. The ductile failure curve presented by Greenwood [11] (a stylized simplification of Johnson's [1] curve) is the basis for the force vs extension profile that will be used as the weld-strength model in this thesis.

The fracture energy of a material is the amount of input energy required to cause the material to fail. According to the ASM Materials Handbook [12], the fracture energy (U_T) can be estimated using the ultimate tensile stress (σ_u), yield stress (σ_0), and the final strain (ϵ_f), as shown in Eqn. 2.13.

$$U_T = \frac{\sigma_0 + \sigma_u}{2}\epsilon_f \tag{2.13}$$

For annealed copper [13], the U_T value is approximately 73 $\frac{MJ}{m^3}$. Because the volume of the weld is already known, a simple multiplication will produce the area that should be accumulated under the force vs extension curve. In this model, it will be assumed that the elastic deformation will account for 5% of the total deformation. This assumption is based on behavior seen in the stress-strain curve from [1] (and shown in Fig. 2.14). With this assumption, the area under the curve and the maximum force can be used to determine the total deformation. The general shape of the force vs extension curve is shown in Fig. 2.15.

The above approximation is for an ideal weld. Due to the stress concentrations and imperfections in the welds that are actually formed at the contacts, the energy required to break them is actually much lower. Therefore, the theoretical energy for the formed weld will be determined then adjusted to a realistic value that accounts for some of these factors. The adjustment factor, α, will modify the theoretical weld-breaking energy to reduce it to a realistic weld-breaking energy, as shown in Eqn. 2.14, where E_{BW} is the energy needed to break a realistic weld, E_{TH} is the theoretical energy needed to break an ideal weld, α is the adjustment factor, and V_W is the volume of the weld (calculated in Section 1.1.2).

$$E_{BW} = \alpha E_{TH} = \alpha U_T V_W \tag{2.14}$$

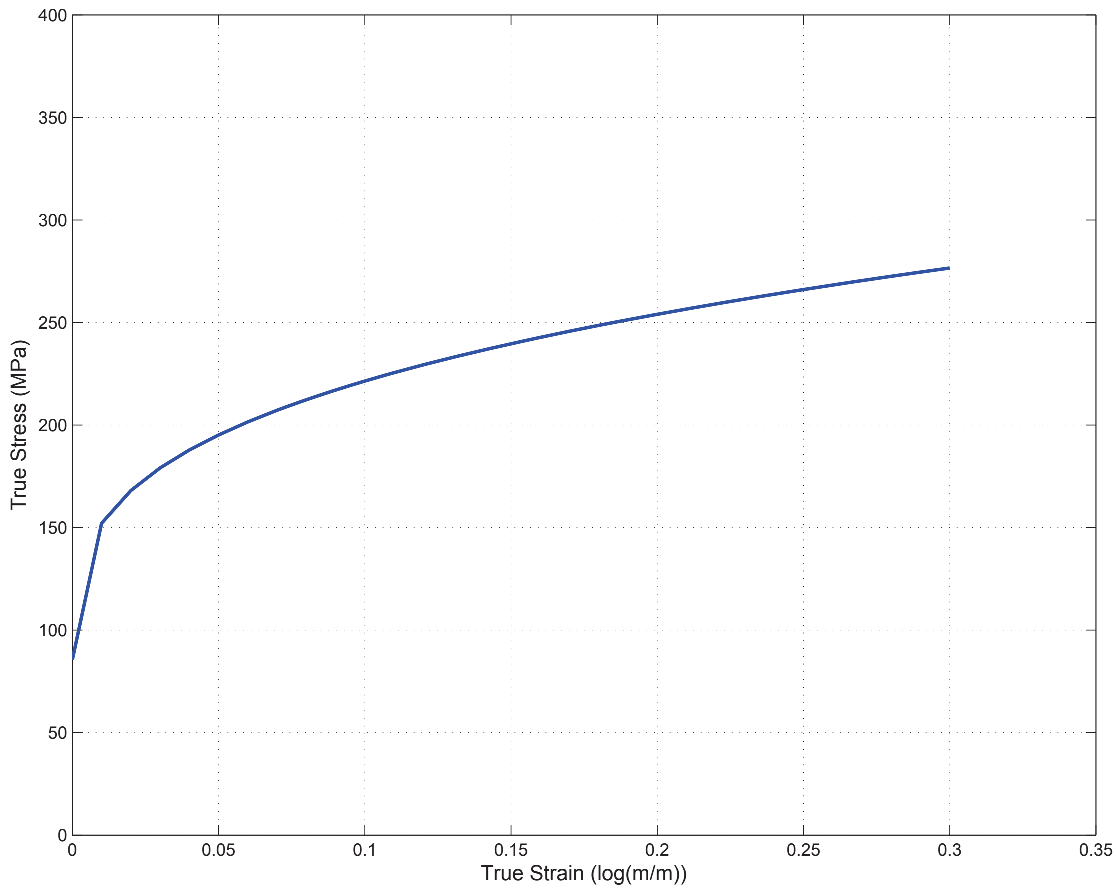

Figure 2.14: Example true stress-strain curve from [1]

Based on prior experience and knowledge of the energy output of the current system, it is hypothesized that the energy required to break a reasonable worst-case-scenario weld is approximately 2.15 J. The dynamic model will be used to simulate a situation in which a reasonable worst-case-scenario weld would be formed, determine the energy required to break this weld, and calculate the α term that will be used to scale the theoretical weld energy to a realistic weld break energy. This term will be calculated in Section 4.3.

2.5 Electrical Interaction Parameters

Section 1.1 presented several electrical interactions in variable form. The purpose of this section is to provide those values along with the appropriate references, as shown in Table 2.5. While the blow-off force and constriction radius equations have been widely documented on a theoretical basis, the same cannot be said for the attractive magnetic force and arc voltage equations. Therefore,

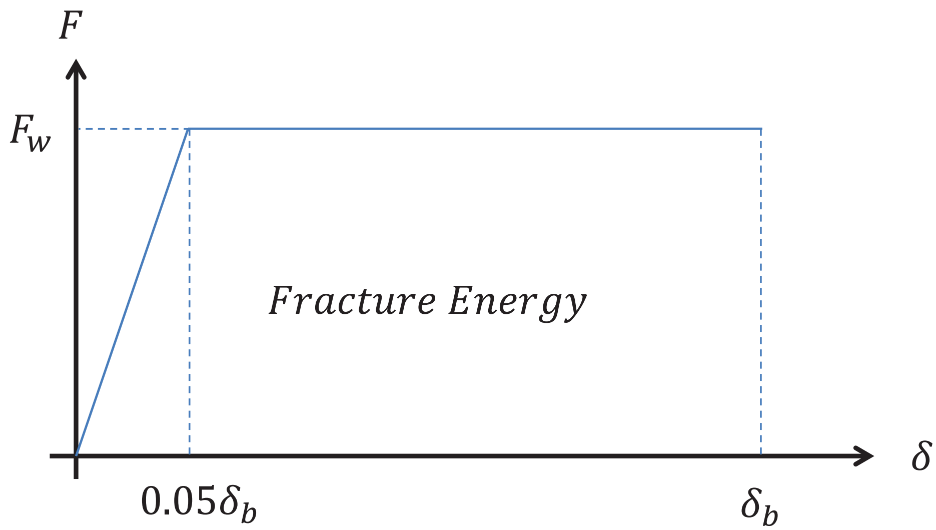

Figure 2.15: The generalized force vs extension curve that defines the weld force as the weld extends.

black-box models previously developed for the interrupters analyzed in this research will be used. It is important to note that these models will not be the same for all interrupters; the values shown are specific to the interrupter that the test was conducted with and should not be assumed to be the same for different designs or ratings.

2.6 Summary

In the above sections, the model parameters have been established and the known values have been denoted. This physical model will now be used to perform a brief energy analysis to challenge the theory that changing the contact pressure spring characteristics can provide additional weld-breaking energy.

Table 2.5: Constants and values used in the equations describing the electrical interactions

Blow-Off Force	Constant	Value
$F_{bo} = 10^{-7} I^2 \ln\left(\frac{R}{r}\right)$	R	22.2 mm
From [2]		
Constriction Radius (r)	Constant	Value
$r = \sqrt{\frac{P}{\pi H}}$	H	$3 \times 10^8 \ \frac{N}{m^2}$
Equation from [2], H-value from [14]		
Attractive Magnetic Force	Constant	Value
$F_{ma} = (A\ (d_o - x_1) + B)\ \frac{I_{rms}^2}{I_{ref}^2}$	A	-560.65 N/m
From [15]	B	32.8 N
	I_{ref}	12.5 kA
Arc Voltage	Constant	Value
$u_a = A + B\ (I_{pk}\ (d_o - x_1)) + C \frac{B_{zmax}}{I}$	A	46.96 V
$+D\ I_{rms} + E\ (\frac{B_{zmax}}{I})^2$	B	0.1528 $\frac{V}{kA\,m}$
From [15]	C	-3.868 $\frac{V\,kA}{mT}$
	D	0.395 $\frac{V}{kA}$
	E	0.139 $\frac{V\,kA^2}{mT^2}$
	$\frac{B_{zmax}}{I}$	10 $\frac{mT}{kA}$

CHAPTER 3

Energy Analysis at Points of Interest

This section shows a method to determine how the energy is transferred through the system during operation. It is often easy to convince oneself that different spring lengths and rates can be utilized to manufacture additional energy during the weld-breaking process. Of course, a simple energy analysis (as is carried out in the following pages) reveals that the only energy that is available to break the weld is that which is provided by the actuator during the full stroke of the closing operation and the overtravel and weld extension lengths of the opening operation. The spring is only the method of storing the energy that is provided by the actuator and releasing it at a rate that the actuator cannot match. In order to help demonstrate this fact, simplicity will be achieved by neglecting the effects of the electrical forces and the energy stored in deflections of the slot ends and the contact surfaces.

3.1 Factors Affecting Weld-Breaking Energy

In order to determine the factors affecting the weld-breaking energy available at the moment of weld breaking a series of energy balances are considered. The energy of the system will be examined at four positions:

- Section 3.1.1: when the system is in the full-open position (State 1)
- Section 3.1.3: when the system is locked in the full-close position (State 2)
- Section 3.1.4: the instant before weld-breaking begins (State 3)

The following sections will examine each situation and present the energy values for each. When formulating potential energy values, the position datum is set at the initial positions of the unattached mass.

3.1.1 Energy at the Full-Open Position

When the system is at the full-open position, the closing force has not yet begun to act and it is assumed that both masses have zero velocity. The total energy in this state (E_1) is given by

$$E_1 = T_1 + V_1 \tag{3.1}$$

where T_1 represents the kinetic energy of the system and V_1 represents the potential energy of the system. It is known that both masses are stationary in this state, so

$$T_1 = 0 \tag{3.2}$$

Evaluating the potential energy is not nearly as easy. In the full open position, energy is stored in the contact pressure spring, the bellows, and the gravitational energy of the attached mass. Therefore, the potential energy V_1 is given by Eqn. 3.3.

$$V_1 = \frac{1}{2}k_{cp}(l_o - l_i)^2 + \frac{1}{2}k_b(l_{bo} - l_{bi} + d_o)^2 + m_1 g(ot) \tag{3.3}$$

Substituting the kinetic and potential energy values into Eqn. 3.1 yields

$$E_1 = \frac{1}{2}k_{cp}(l_o - l_i)^2 + \frac{1}{2}k_b(l_{bo} - l_{bi} + d_o)^2 + m_1 g(ot) \tag{3.4}$$

Now that the energy at the full-open position is known, the next step is to determine work done on the system between the full-open and full-close positions.

3.1.2 Work Done Between Full-Open and Full-Close Positions

The total work done in the energy change is made up of the work done by the closing force, because the electrical effects and losses have been neglected.

$$W_{12} = F_C(d_o + ot) \tag{3.5}$$

The addition of this work to the system when in the full-open state will produce the system in the full-close state, which is described below.

3.1.3 Energy at the Full-Close Position

Following the same procedure as above, the energy of the system in the full-close position (E_2) is given by the combination of the kinetic and potential energies:

$$E_2 = T_2 + V_2 \tag{3.6}$$

Once again, the attached and unattached masses are both stationary, so

$$T_2 = 0 \tag{3.7}$$

Potential energy is stored in the contact pressure spring, the bellows, and both masses. Therefore, the potential energy V_2 is given by Eqn. 3.8.

$$V_2 = \frac{1}{2}k_{cp}(l_o - l_i + ot)^2 + \frac{1}{2}k_b(l_{bo} - l_{bi})^2 + m_1 g(d_o + ot) + m_2 g(d_o + ot) \tag{3.8}$$

Substituting the kinetic and potential energy values into Eqn. 3.6 yields

$$E_2 = \frac{1}{2}k_{cp}(l_o - l_i + ot)^2 + \frac{1}{2}k_b(l_{bo} - l_{bi})^2 + m_1 g(d_o + ot) + m_2 g(d_o + ot) \tag{3.9}$$

The principle of work-energy states that

$$E_1 + W_{12} = E_2 \tag{3.10}$$

Substituting Eqns. 3.4, 3.5, and 3.9 into Eqn. 3.10 yields Eqn. 3.11.

$$\frac{1}{2}k_{cp}[(l_o - l_i + ot)^2 - (l_o - l_i)^2] = F_C(d_o + ot) - m_1 g d_o - m_2 g(d_o + ot) + \frac{1}{2}k_b[(l_{bo} - l_{bi} + d_o)^2 - (l_{bo} - l_{bi})^2] \tag{3.11}$$

This equation will be used later to make the weld-breaking energy dependence on the closing force explicit.

3.1.4 Energy Immediately Before Weld-Breaking Process Begins

Assuming a relatively short weld extension, the energy available to break the weld is the quantified as the system's kinetic energy the instant before the weld-breaking process begins. The potential energy stored in the full-close position (V_2) was already determined, so now the potential energy before the weld-breaking process must be determined (V_3). For completeness, the total energy (E_3) will be calculated, as before.

$$E_3 = T_3 + V_3 \tag{3.12}$$

In this case, the attached mass is still (roughly) stationary, while the unattached mass has some velocity. Therefore, the kinetic energy is given by Eqn. 3.13.

$$T_3 = \frac{1}{2}m_2\dot{x}_2^2 \tag{3.13}$$

The potential energy in this state is still stored by the contact pressure spring, the bellows, and both masses as shown here in Eqn. 3.14.

$$V_3 = \frac{1}{2}k_{cp}(l_o - l_i)^2 + \frac{1}{2}k_b(l_{bo} - l_{bi})^2 + m_1 g(d_o + ot) + m_2 g(d_o) \tag{3.14}$$

Therefore, the total energy is given as

$$E_3 = \frac{1}{2}m_2\dot{x}_2^2 + \frac{1}{2}k_{cp}(l_o - l_i)^2 + \frac{1}{2}k_b(l_{bo} - l_{bi})^2 + m_1 g(d_o + ot) + m_2 g(d_o) \tag{3.15}$$

As the spring is accelerating the mass, the opening force is also acting on the system, so the work done must be calculated. The work done by this force is outlined in the next section.

3.1.5 Work Done Between Full-Close Position and the Instant Before the Weld-Breaking Process Begins

During the travel between the full-close and weld-break-start positions the work term is made up of only the work done by the opening force (F_O) as shown in Eqn. 3.16.

$$W_{23} = F_O(ot) \tag{3.16}$$

Now that the work done between State 2 and State 3 is known, the energy available to break the weld can be determined. This calculation will be done in the next section.

3.1.6 Energy Available to Break the Weld

The energy available to break the weld can be quantified as the energy stored in the kinetic energy of the unattached mass. The basic equation for changes in energy levels is provided in Eqn. 3.17. Rearranging this equation to solve for the T_3 term yields the energy available to break the weld, E_A, as shown in Eqn. 3.18.

$$E_3 = E_2 + W_{23} \tag{3.17}$$

$$E_A = T_3 = E_2 + W_{23} - V_3 \tag{3.18}$$

Substituting Eqns. 3.9, 3.14, and 3.16 into Eqn. 3.18 yields the following equation for the available weld energy in terms of the system values.

$$E_A = \frac{1}{2}k_{cp}(l_o - l_i + ot)^2 + \frac{1}{2}k_b(l_{bo} - l_{bi})^2 + m_1 g(d_o + ot) + m_2 g(d_o + ot)$$
$$+ F_O(ot) - \frac{1}{2}k_{cp}(l_o - l_i)^2 - \frac{1}{2}k_b(l_{bo} - l_{bi})^2 - m_1 g(d_o + ot) - m_2 g(d_o) \quad (3.19)$$

The substitution of the work done by the closing force (Eqn. 3.11) yields

$$E_A = F_C(d_o + ot) + F_O(ot) + \frac{1}{2}k_b[(l_{bo} - l_{bi} + d_o)^2 - (l_{bo} - l_{bi})^2] - m_1 g(d_o) - m_2 g(d_o) \quad (3.20)$$

Out of the terms in the above equation, the only two substantial terms are those that are contributed by the closing force and the opening force provided by the actuator. Therefore, adjusting the actuator forces, the initial contact gap, and overtravel can allow one to approximate the energy available to break the weld. The above calculation can be used to determine the approximate system characteristics, then the dynamic model developed in this work can be used to fine-tune the system.

3.2 Discussion

Utilizing an energy perspective for this analysis is helpful because it removes the distance and time dependence that causes confusion when looking at forces. Clearly, the closing force times the mechanism stroke represents a substantial amount of the energy that is being stored in the spring. Upon opening, a stiff spring with a small compression will be able to provide the same amount of energy as a weak spring with a large compression – that is the energy provided to the spring by the actuator. The spring rate and lengths should be changed only for the purposes of achieving the proper "contact pressure force." The energy to break the weld must be determined, so that the required amount of stored energy can be adjusted by changing the actuator force (and changing the . It is essential that it is understood that the spring is merely a method of storing the energy supplied by the actuator.

CHAPTER 4

Parameter Identification

Now that the mathematical model has been created, the proper values for the constants utilized by the model must be identified. The parameters identified for further testing are

- the $\frac{E}{\beta}$ term that dictates when arcing begins, as described in Section 1.1.1
- the spring/damper pair used to model the contact between the fixed contact and the attached mass (k_{fc}, c_{fc})
- the weld-breaking energy adjustment factor (α)

The following sections outline the methods used to identify these parameters and the results.

4.1 Determination of Parameters Predicting Dielectric Breakdown and Recovery

As discussed in Section 1.1.1, dielectric breakdown is thought to occur when some critical electric field value is reached, while considering any field enhancements β (shown in Eqn. 4.1).

$$E_C = \frac{\beta U}{d} \tag{4.1}$$

While neither the E_C or β values are known, the real value of interest here is the β term, which is thought to change with the contact gap. However, the calculation of this value is difficult because it requires the characterization of the surface profile of the contact face (for the β_m term). Also, the calculation of the β_g term (accounting for the shape of the contact) is not known for the contacts in use. Therefore, rather than attempting to characterize β through calculation, an empirical approach was adopted.

This empirical approach involved dividing Eqn. 4.1 by the β term, yielding Eqn. 4.2.

$$\frac{E_C}{\beta} = \frac{U}{d} \tag{4.2}$$

When examining test data, the voltage U and gap d values can be determined at the moment of breakdown (when arcing starts) and recovery (when arcing stops). Therefore, the enhanced electric field could be determined as a function of voltage and contact gap, which are both outputs of the dynamic model. The following subsections outline this process and the results.

4.1.1 Methods

Data from a standard duty cycle test data was obtained to determine this E/β value. These duty cycle tests were measuring the performance of an ACR called a triple-single. Triple-singles are made up of three individual ACRs that are each responsible for interrupting one of the three phases of power utilized in power distribution grids. These particular duty cycle tests included 38kV and 27kV operations at fault currents corresponding to ANSI C37.60. Instantaneous voltage and current curves for each phase as well as a single curve for the position of the unattached mass are provided for each operation. No position data is available for the attached mass because it is at high voltage for these tests. However, the overtravel for the ACR is known, so the contact gap can be determined to be the position of the unattached mass minus the overtravel (assuming that there is no additional compression of the contact pressure spring beyond the preload during the approach phase). Several test series were run, with a single test series being composed of four pairs of close-open operations.

Large voltage spikes are often seen in the voltage signal during dielectric breakdown and recovery. These large spikes are often much higher than the amplitude of the sinusoidal line voltage, but provide an excellent method of determining at what time a dielectric event (breakdown or recovery) has occurred. However, the recorded voltage data does not give a good approximation of the input voltage at this time because of the aforementioned spike. Therefore, the voltage signal was rebuilt using the *nlinfit* function of MATLAB to create a fitted voltage curve (Step 2 of the program flowchart, shown in Fig. 4.1). The voltage values used in these tests are the ones determined from the fitted voltage curve, rather the

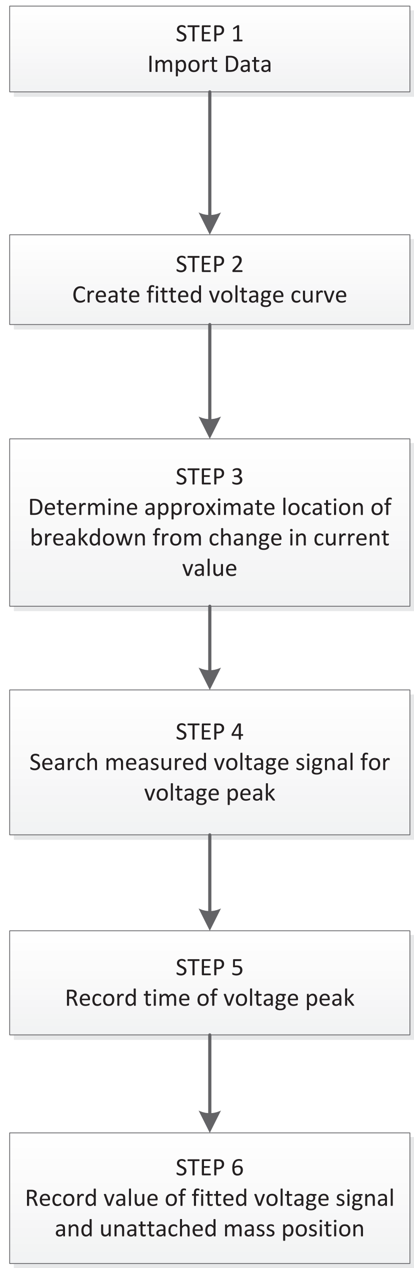

Figure 4.1: Flowchart of the program used to find the voltage and unattached mass position values at breakdown

actual measured voltage curves.

The approximate time that arcing starts was determined (Step 3) by the change from zero current to some appreciable value (above the noise level, generally 50-100 A). This value is marked with a light green asterisk (for breakdown) or a red asterisk (for recovery). The recorded voltage wave was then searched for one of the aforementioned peaks around this approximate time (Step 4). Once this peak value

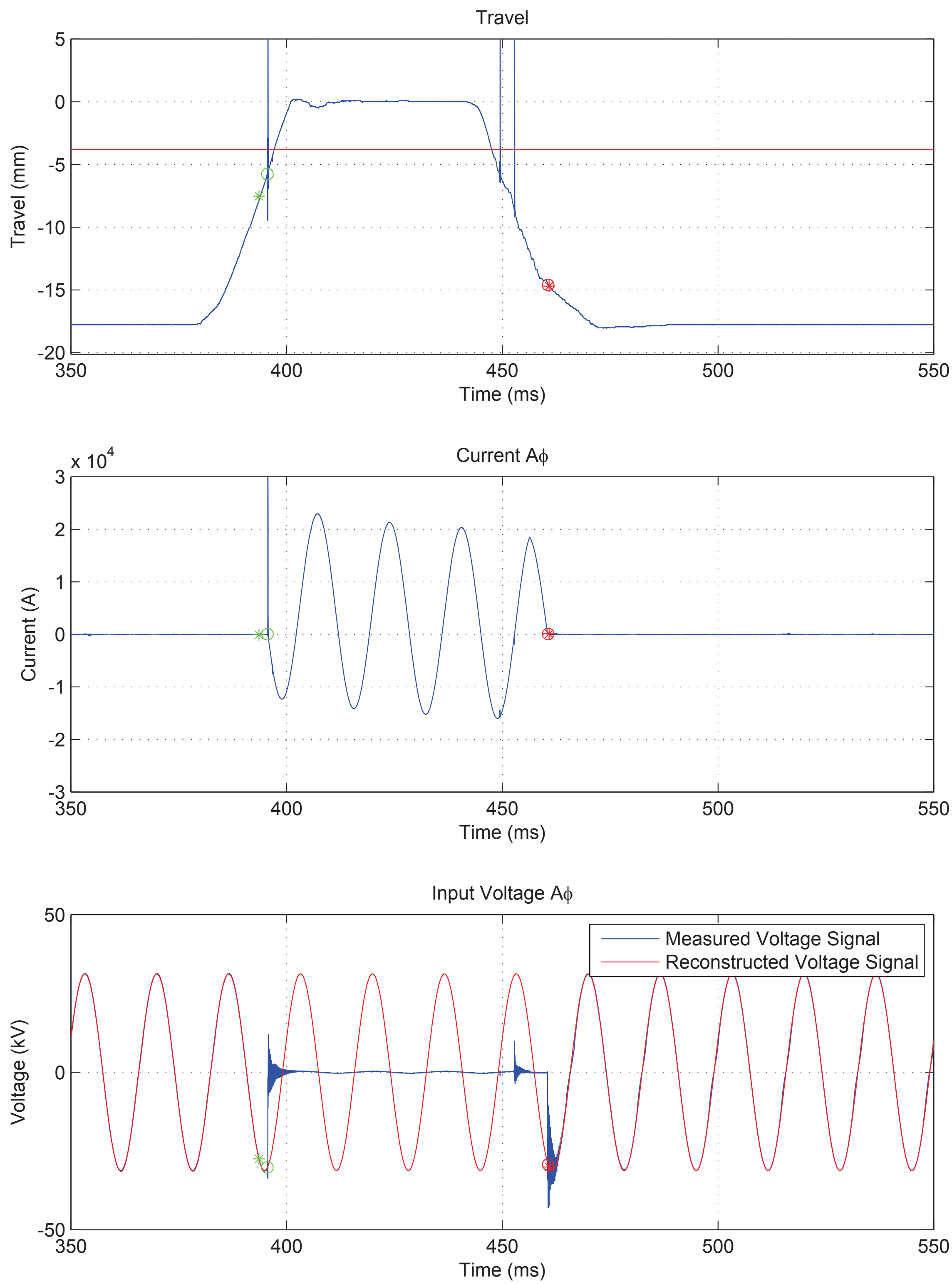

Figure 4.2: Sample travel, current, and voltage plots showing the values recorded for dielectric breakdown (green) and dielectric recovery (red). The asterisks represent the approximate time that arcing started/stopped as determined from the current data. The circles represent the more precise times determined based on the peaks in the voltage data. The ϕ term identifies which phase the plotted data is from (in this case it was A-Phase).

was found, the time was recorded (Step 5). The value of the fitted voltage signal and the position of the unattached mass was recorded at the determined time (Step 6, marked with light green or red circles for breakdown or recovery, respectively).

4.1.2 Results

The method outlined in Section 4.1.1 was repeated for several open and close operations and the result was a table of voltage, gap, and E/β (calculated as $\frac{voltage}{gap}$) values. It was expected that the E/β value at breakdown would vary with respect to gap, so the E/β vs gap plots were examined. Both opening and closing operations will be examined, starting with the closing operation. It is important to note that the overtravel length can change due to plastic deformation of the lost motion mechanism slot, thus resulting in the actual contact gap being somewhat ambiguous. This might be the cause of some of the noise that will be seen in the following plots.

Closing Operation Results

The plot of the E/β values as a function of the contact gap for the closing operations is shown in Fig. 4.3. The plot shows an upper envelope and another curve that appears to cut through the upper two-thirds of the data. However, it was expected that a lower envelope would be seen, representing the values of E/β above which breakdown should occur. The plot shows considerably different behavior.

It is known that there are some interactions between the phases in a three-phase system. It is hypothesized that once the first phase experiences dielectric breakdown due to high voltage levels and small gaps, then the other two phases are also forced to break down, despite relatively low voltage levels. In order to test this hypothesis, the phase with the largest E/β value was isolated for each test, resulting in a third of the points shown in the earlier plot (Fig. 4.3). This plot, shown in Fig. 4.4, shows a clear pattern of two curves that are roughly $\frac{1}{gap}$ relations. The upper curve represents the tests done at approximately 38 kV and lower curve corresponds to the tests done at approximately 27 kV. It does not appear that there is any dependence on the level of fault current and that no breakdown occurs before a gap of approximately 2.75 mm for either voltage. It is believed that this curve represents the E/β value that a single phase unit would breakdown at and is used

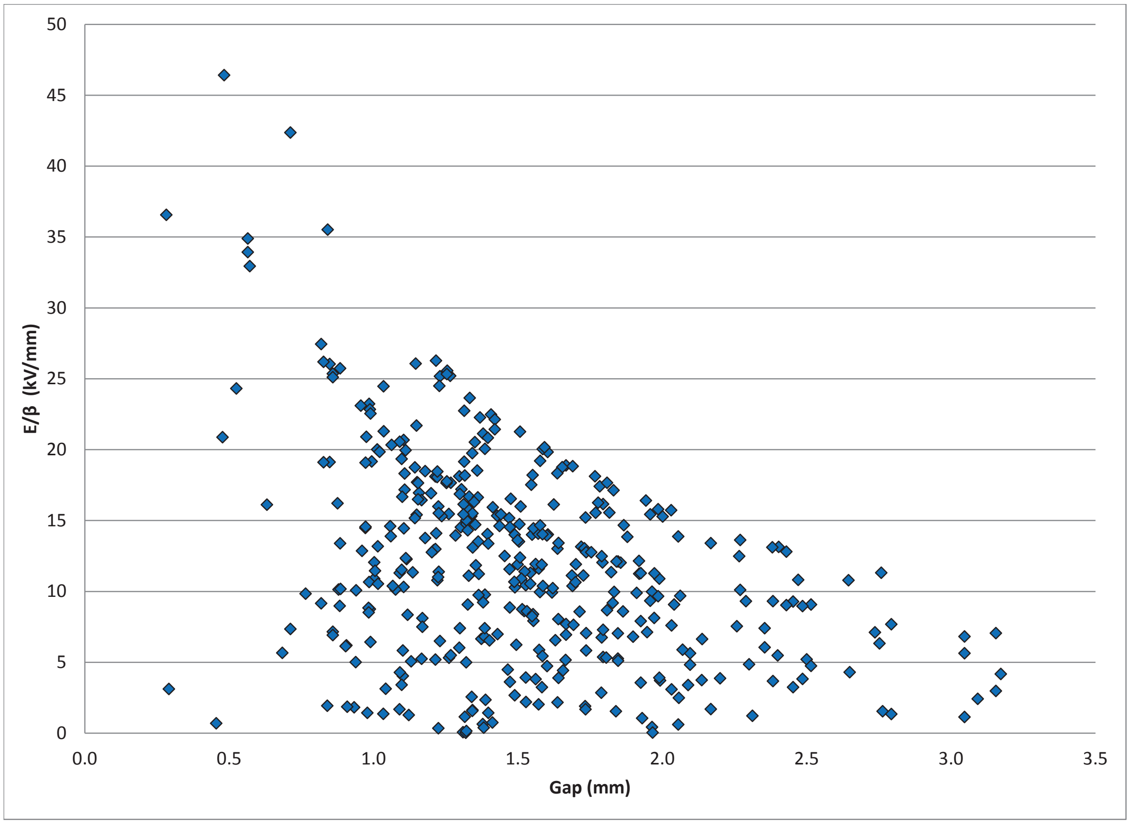

Figure 4.3: E/β vs gap for all phases of every closing operation

in the model to determine when arcing starts.

It is important to note that the $\frac{1}{gap}$ relationship when plotted as a function of gap indicates that breakdown occurs at 30.5 kV and 21.1 kV regardless of the gap between the contacts. This result is *not* what was expected because generally breakdown has been historically thought of in terms of electric field strength. That is, breakdown could occur at a large voltage and a large gap, but not at a slightly smaller gap if the voltage was significantly smaller. The data indicates that breakdown is based on voltage rather than electric field, as shown in Fig. 4.5. However, this could also indicate that the β term increases as gap decreases, and that the higher β value balances the smaller gap. This question does not affect the current research, but is an interesting avenue for further discussion and discovery.

Further examination of the plot shown in Fig. 4.4 reveals that the breakdown always occurred at the maximum value of the voltage wave. The values shown in the legend represent the rms line-to-line voltage. Dividing this value by $\sqrt{3}$ yields the rms line-to-ground voltage. Multiplying this value by $\sqrt{2}$ yields the

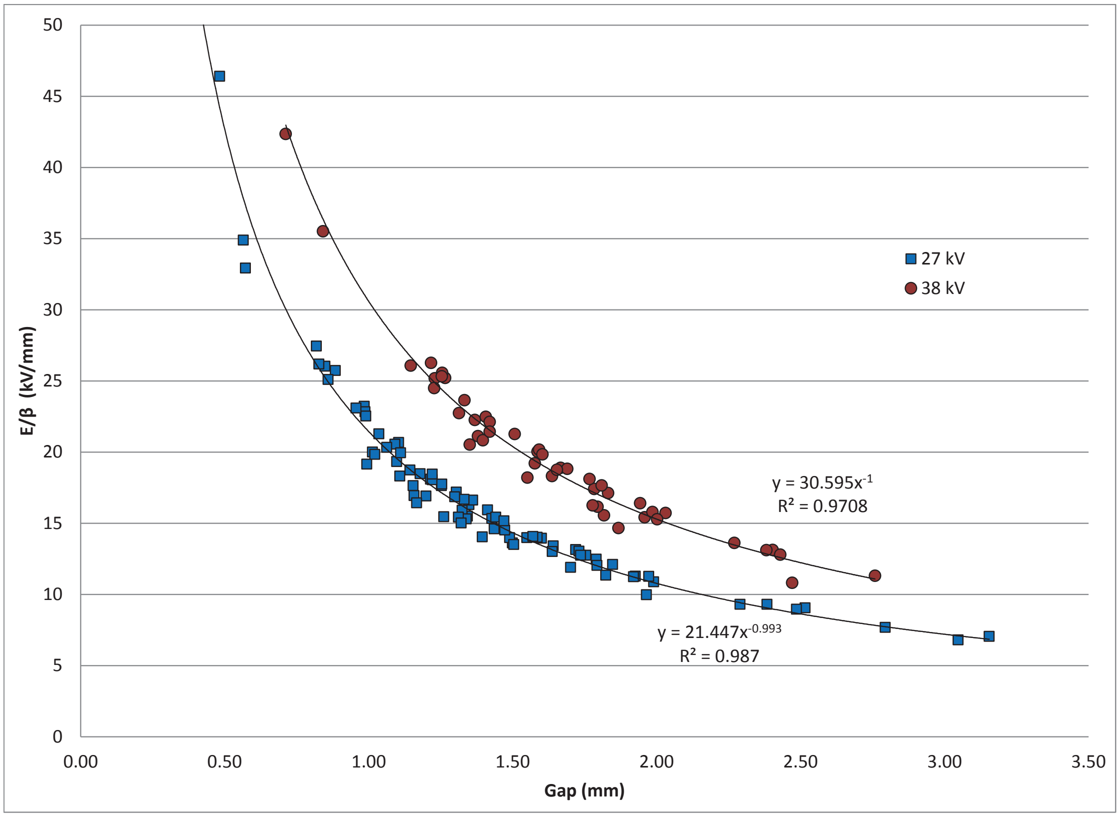

Figure 4.4: The maximum E/β value for each phase of each closing operation plotted as a function of contact gap

peak value of the voltage wave, as seen in the coefficient of the fit in Fig. 4.4. This discovery is an interesting development, because it implies that the breakdown voltage does not depend on the contact gap. Rather than a complex breakdown model based on the electric field strength, the model must merely look for a voltage maximum after a critical gap (2.75 mm) is reached. This simple approach is the breakdown model used in the dynamic model.

Opening Operation Results

A similar approach was taken with the E/β values from the opening operations. Figure 4.6 shows a much tighter collection of points, but there is still considerable noise at the larger gap values. Once again, the largest E/β value was selected from each operation and only those values were plotted as a function of contact gap. This plot, shown in Fig. 4.7 shows another relationship that is very close to being inversely proportional to the contact gap (as seen by the power value

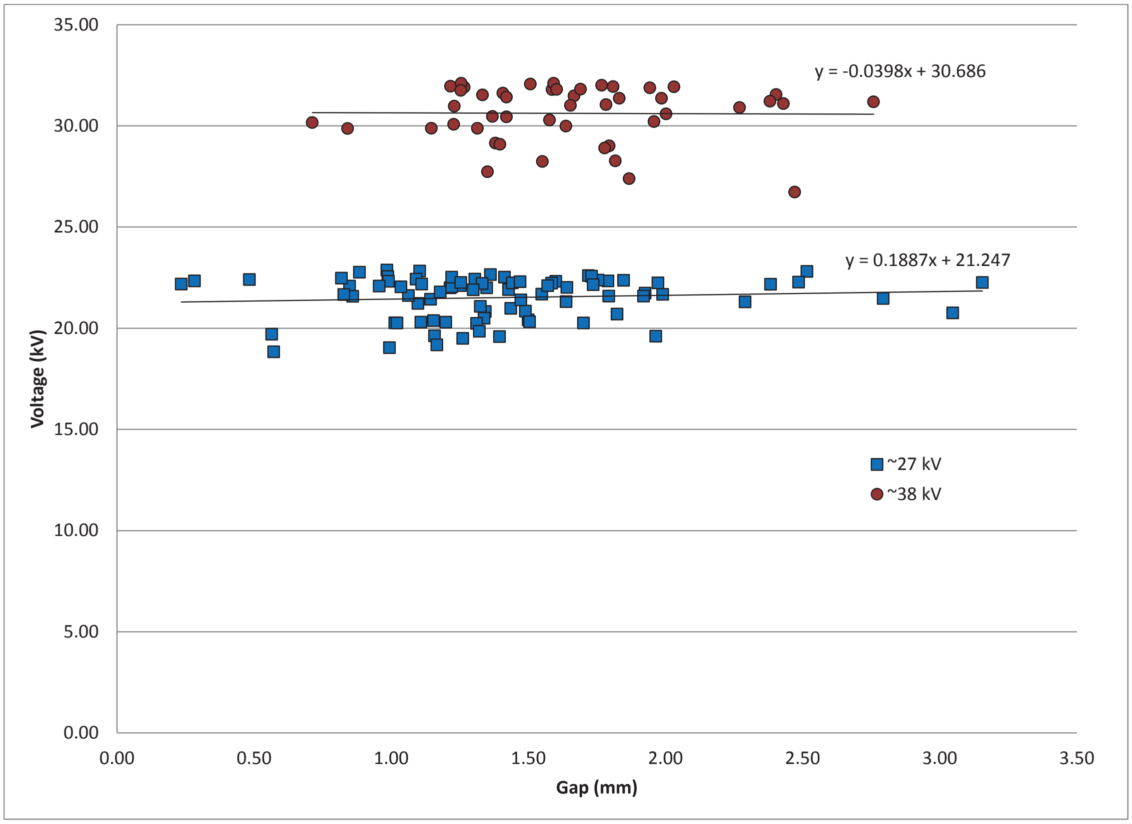

Figure 4.5: The maximum voltage value for each phase of each closing operation plotted as a function of contact gap, showing the lack of voltage-dependence on gap.

being very close to -1). This holds true for both the 27 kV and 38 kV voltage ratings.

As with the closing operation, further examination of Fig. 4.7 reveals that arcing always stopped when the voltage wave had reached its peak (as seen by the coefficients of the power fits, 31 and 23, which are very close to the voltage wave peaks for 38 kV and 27 kV tests, respectively). Therefore, dielectric recovery will be determined to occur at the first voltage peak after some critical gap (2 mm) has been reached. This approach is the recovery model used in the dynamic model.

4.2 Determination of Spring/Damper Values for Contact Model Between the Fixed and Moveable (Attached Mass) Contacts

As discussed in Chapter 2, the Kelvin-Voight model will be used to represent the interactions between the fixed contact and the attached mass. In order to determine the spring/damper values in the model, the closing process was viewed

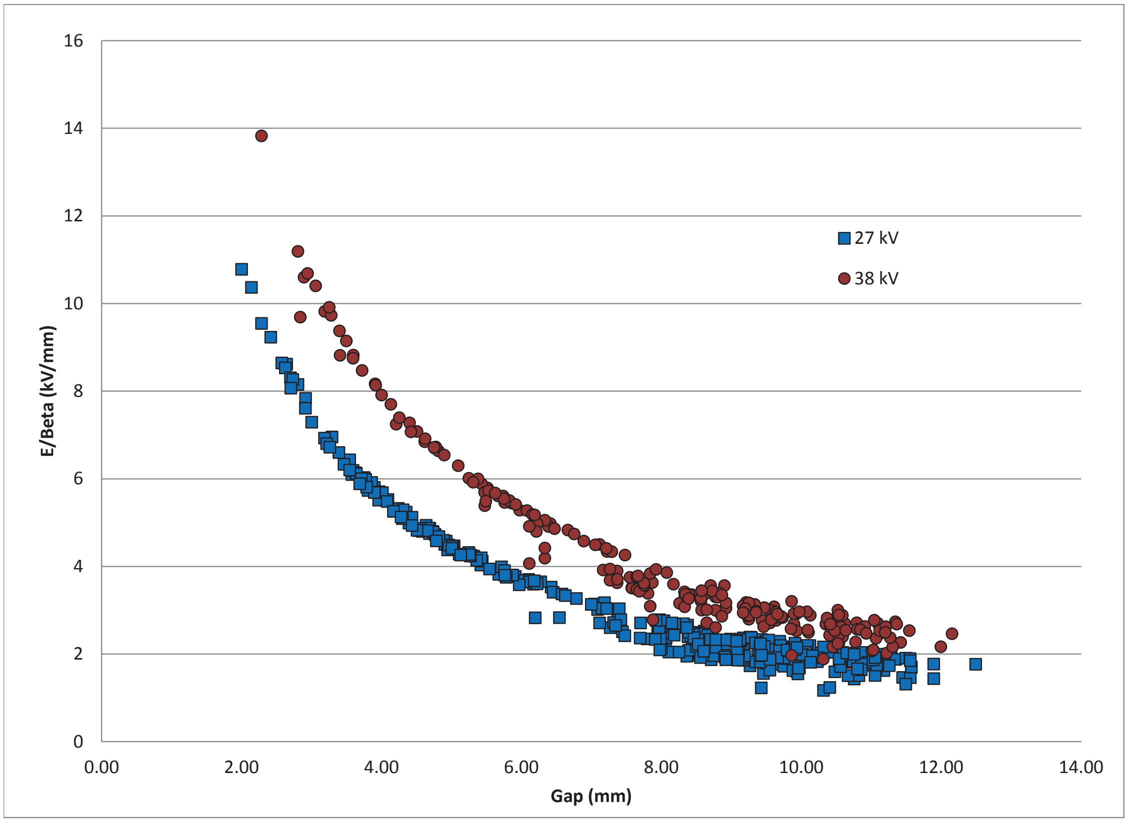

Figure 4.6: The E/β value for each phase of each opening operation plotted as a function of contact gap

with a high speed camera. The attached mass is normally not visable due to the epoxy encapsulation that surrounds and insulates the high-voltage components, so a special ACR had to be constructed. A slot was cut in the current exchange, then filled with a wood plug and covered in a curved wood block that was contoured to the current exchange, as shown in Fig. 4.8. The wooden plug and block prevented epoxy from leaking into the current exchange while also ensuring that there would be a hollow part in the final molded part (Fig. 4.9). After the molding process was complete, the thin layer of epoxy over the wood block was milled out and the wood block and plug were removed. This process created a window into the ecap for high-speed camera viewing of the attached mass during the closing process, as shown in Fig. 4.10.

The contact bounce was examined in two ways, both of them utilizing the modified ACR that was described above. The first set of tests involved an examination of the motion of the attached mass during closing operations. This test

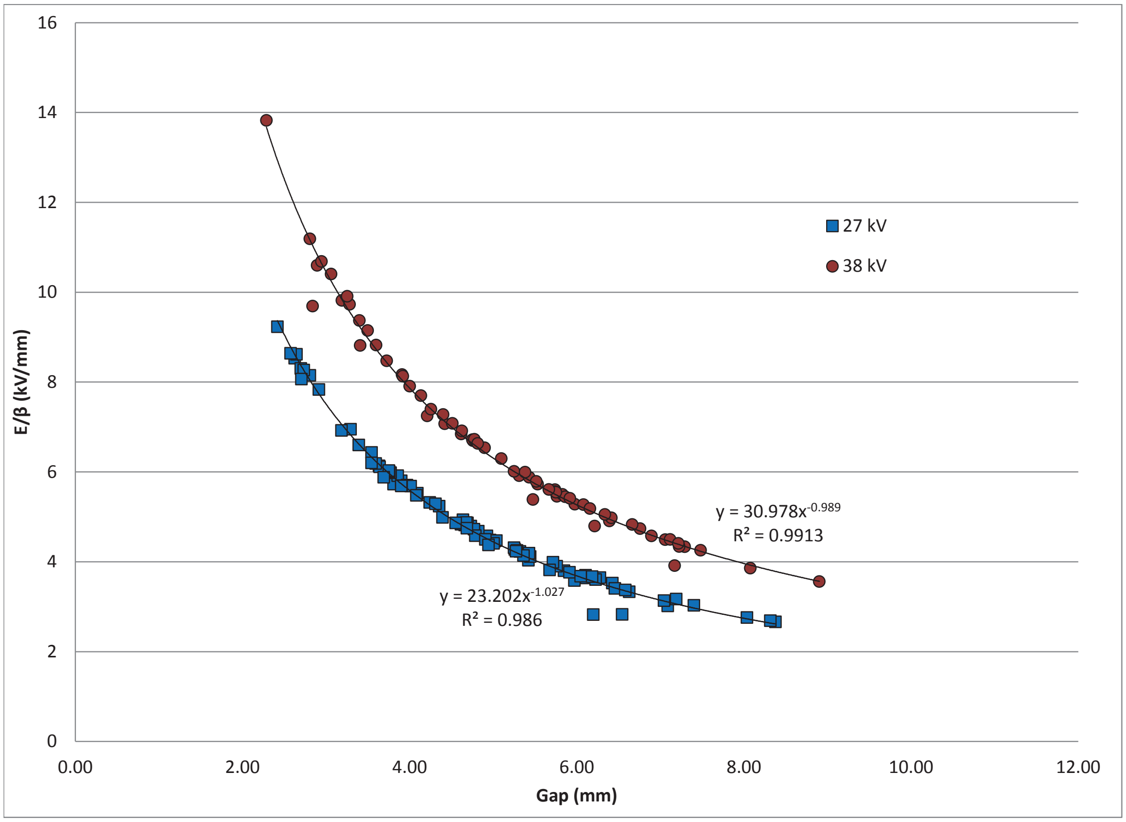

Figure 4.7: The maximum E/β value for each phase of each opening operation plotted as a function of contact gap

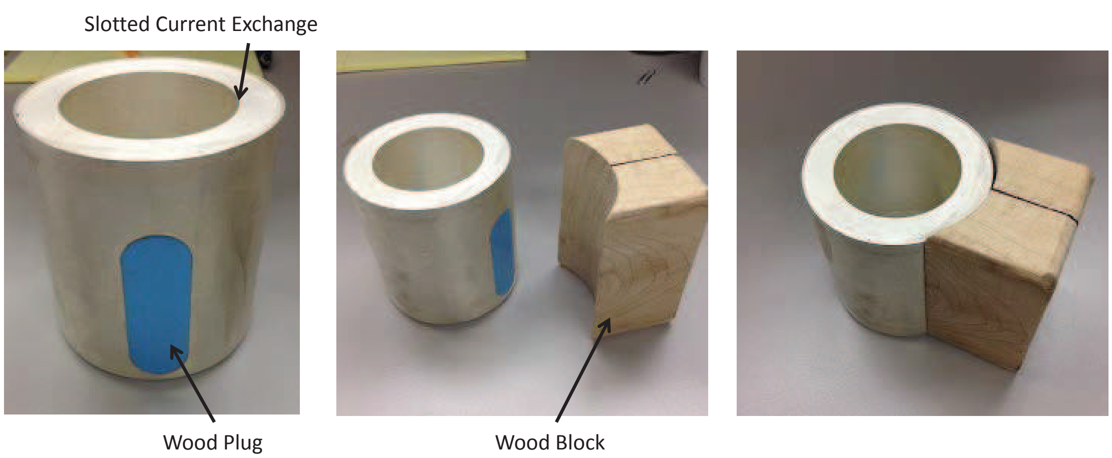

Figure 4.8: Slotted current exchange with wood plug and block.

was done by recording several operations utilizing a high speed camera. This high speed data was then analyzed with tracking software in order to determine the travel. The results of four of the tests are shown in Fig. 4.11. There is some variation between the trials. This variation is most likely due to tolerances in the

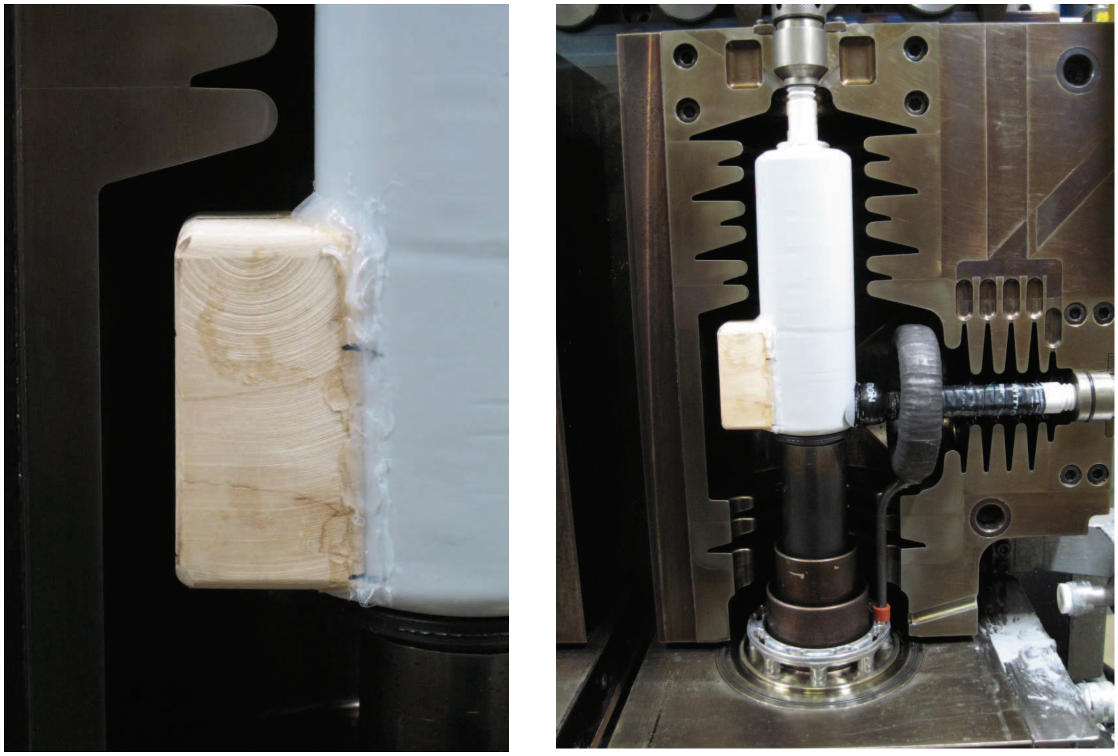

Figure 4.9: Slotted current exchange with wood plug and block installed for molding.

system that are brought out by the violence of the collision at the end of the closing operation. Each of these tests most likely stopped at the same point, but the travel values were based on their initial positions, meaning that this is reflecting the different initial position.

Due to the noise in the signal, additional tests were done to ensure that the contacts have actually lost electrical continuity. For this purpose, a small voltage (5 V) was applied across the terminals of the same ACR as was used for the above test. The voltage across the terminals was measured with an oscilloscope during the closing operation. The oscilloscope would read 5 Volts when the contacts are touching and 0 Volts when the contacts have lost electrical continuity. The results from 11 of these tests were recorded and overlayed on one another, as shown in Fig. 4.12. Good consistency is seen among the trials, showing three bounces of varying size.

In order to determine the time and magnitude of the bounces, the data sets were combined. The oscilloscope data from Trial 0 was overlayed on top of the travel data from the high speed camera recordings. The time of the make-break

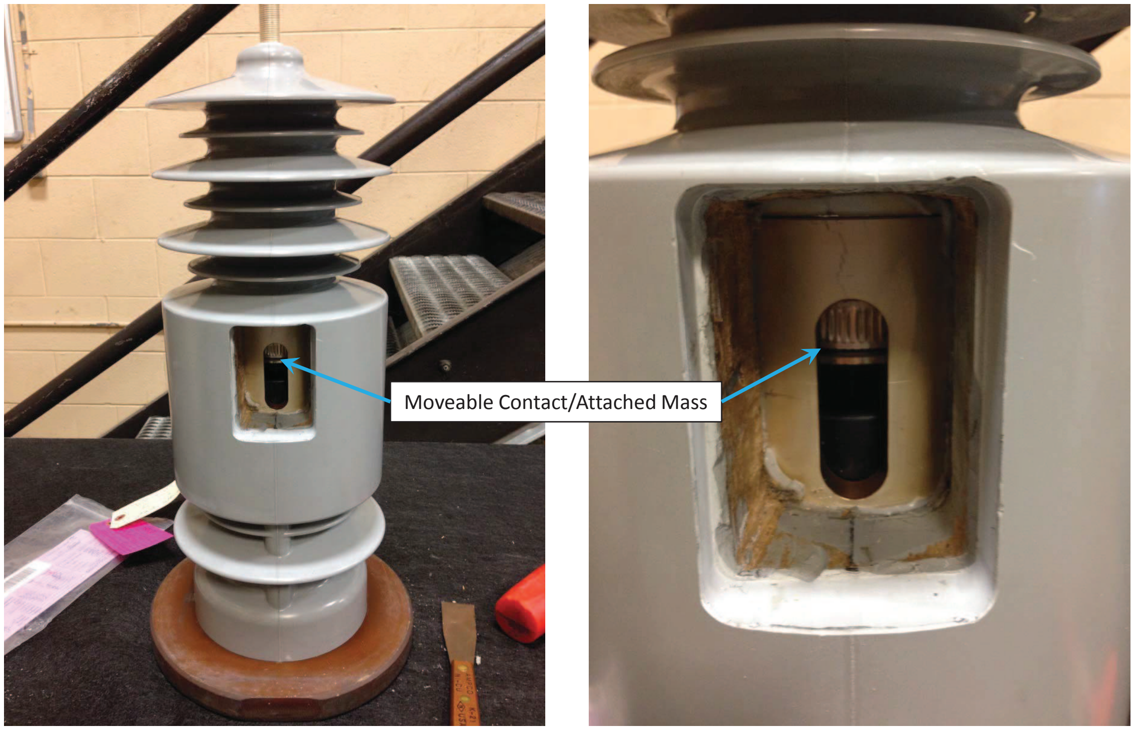

Figure 4.10: ACR with viewing window and view of the attached mass.

data has been shifted by hand to a position that centers the first bounce on the make-break data with that of the position data. A plot of this overlay that is enlarged to show the area of interest is shown in Fig. 4.13.

It is clear from Fig. 4.13 that the amount of time spent bouncing after the first bounce is relatively small. The strongest possible weld will occur when the pre-strike arcing occurs at the largest gap due to the large amount of energy that is input to the contacts during this time. When the pre-strike occurs at the earliest point, the amount of additional energy imparted to the contacts due to the second and third bounce is relatively small. With respect to time, the second and third bounce provide an additional 7% of time during which arcing occurs. Also, because the voltage and current waves must be at a peak for pre-strike arcing to occur, the later bounces contribute even less so to the energy imparted to the contacts ($< 2\%$). For this reason and to increase the simplicity of the system for the purpose of expediting the optimization of the spring/damper sizes, only the first bounce will be considered.

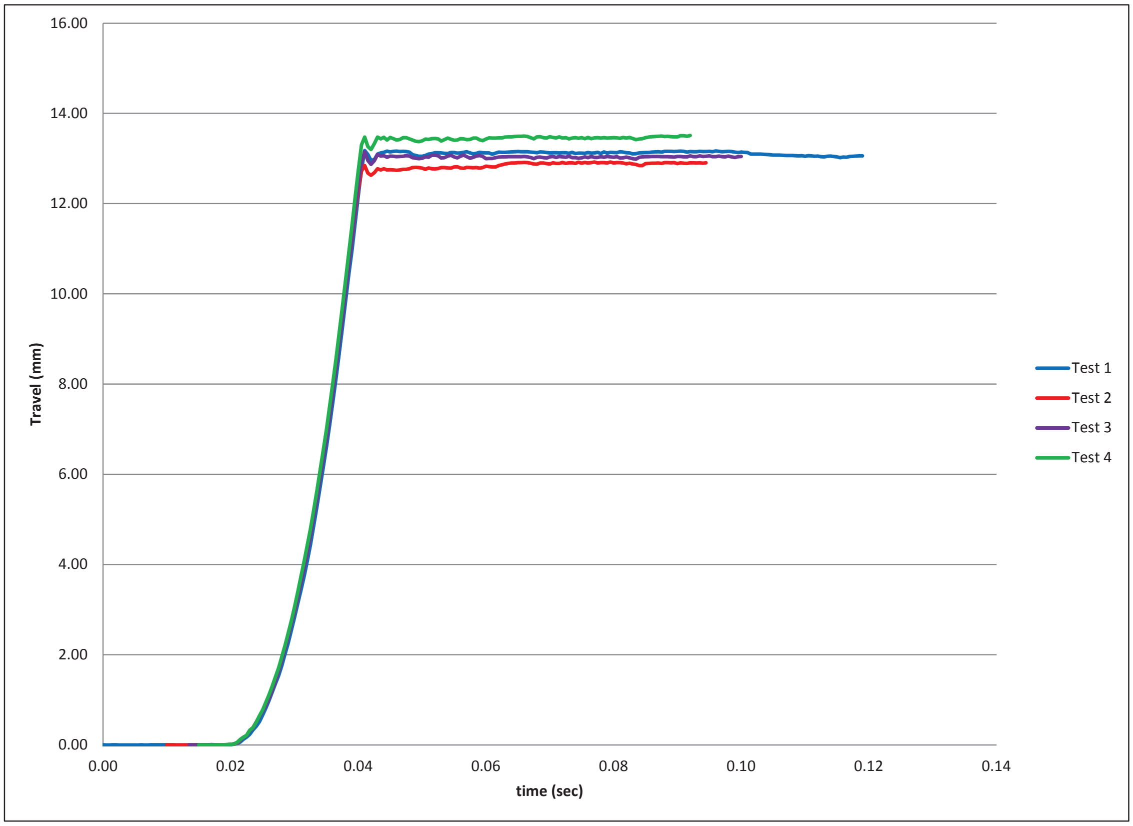

Figure 4.11: Closing operation travel traces from analyzed high speed camera recording.

4.2.1 Results

The sizing of the spring/damper pair was completed using MATLAB's *fmincon* function. It is a constrained optimization routine that is attempting to minimize an objective function. In this case, the object function was chosen to be the square of the error between the simulated motion of the attached mass and the travel trace obtained above for the first bounce. As shown below in Eqn. 4.3

$$\begin{aligned} &min && \sum_{i=855}^{1000}\left[x_{1sim}\left(\frac{.02}{1000}i\right)-x_{1bounce}\left(\frac{.02}{1000}i\right)\right]^2 && (4.3)\\ &subject\ to && 10^{-4}N/m \le k_{fc} \le 10^{9}N/m && i=1,...,1000\\ & && 10^{-6}Ns/m \le c_{fc} \le 10^{4}Ns/m && i=1,...,1000 \end{aligned}$$

Utilizing this optimization, it was found that the optimal spring/damper pair

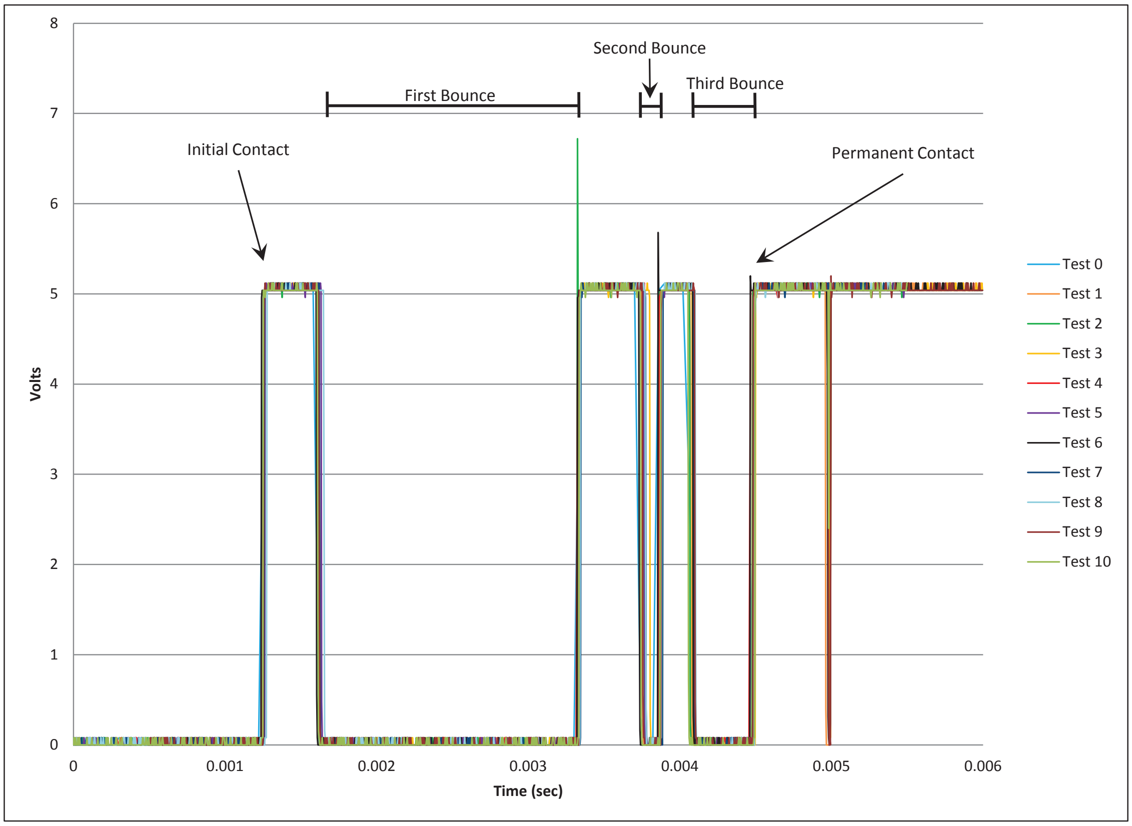

Figure 4.12: Oscilloscope measurements showing contact bounce.

has the values $k_{fc} = 4.5 \times 10^7 N/m$ and $c_{fc} = 3.7 \times 10^3 Ns/m$. When these values are used, the resulting performance is shown in Fig. 4.14. There is clearly some difference between the high speed camera data and the model results. This difference is due to the fact that a fairly simple model is used. Adding additional factors into the contact model would produce higher fidelity, as discussed in Section 5.2.

4.2.2 Alternate Model Variations

The model outlined above was not the only model examined. As mentioned above, a linear one-way damper was utilized. The use of a nonlinear damper (that had a penetration-dependent damping coefficient) and a two-way damper were also considered, both separately and in conjunction with one another. First, when the nonlinear damper was used, a very large spring rate was required to prevent unrealistic penetration into the fixed contact, thus storing a large amount of energy in the spring. During restitution, the bounce amplitude is considerably higher than

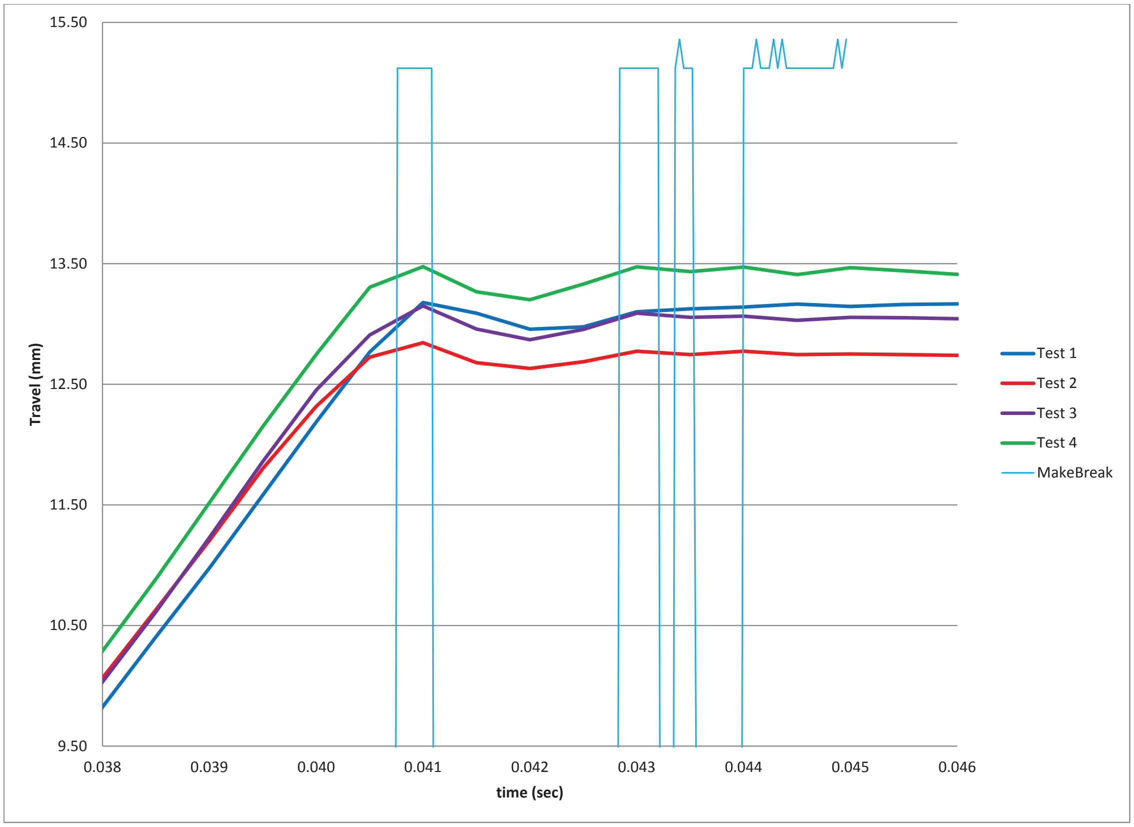

Figure 4.13: Enlarged plot of make-break data overlayed with the travel traces from the high speed camera data.

the experimental data shows and the second contact point occurs much earlier than the experimental data shows. Secondly, when the two-way damper was used, the response on restitution was much too slow to replicate the response seen in the experimental data. It is important to note that the objective function was not changed during the evaluation of these model variations. The performance of these alternatives should be considered when pursuing future models.

4.3 Weld-Break Energy Adjustment Factor

In Sections 1.1.2 and 2.4, the method for determining the weld strength based on the amount of energy input to the contact during arcing was established. Based on the worst-case scenario for arcing (arcing starts at $x_1 = d_o - 2.75\ mm$, the largest possible gap), the total energy transferred into the contacts is approximately 1300 J. Based on the aforementioned equations and assuming that the contact begins at room temperature (295.15 K), this amount of energy would melt

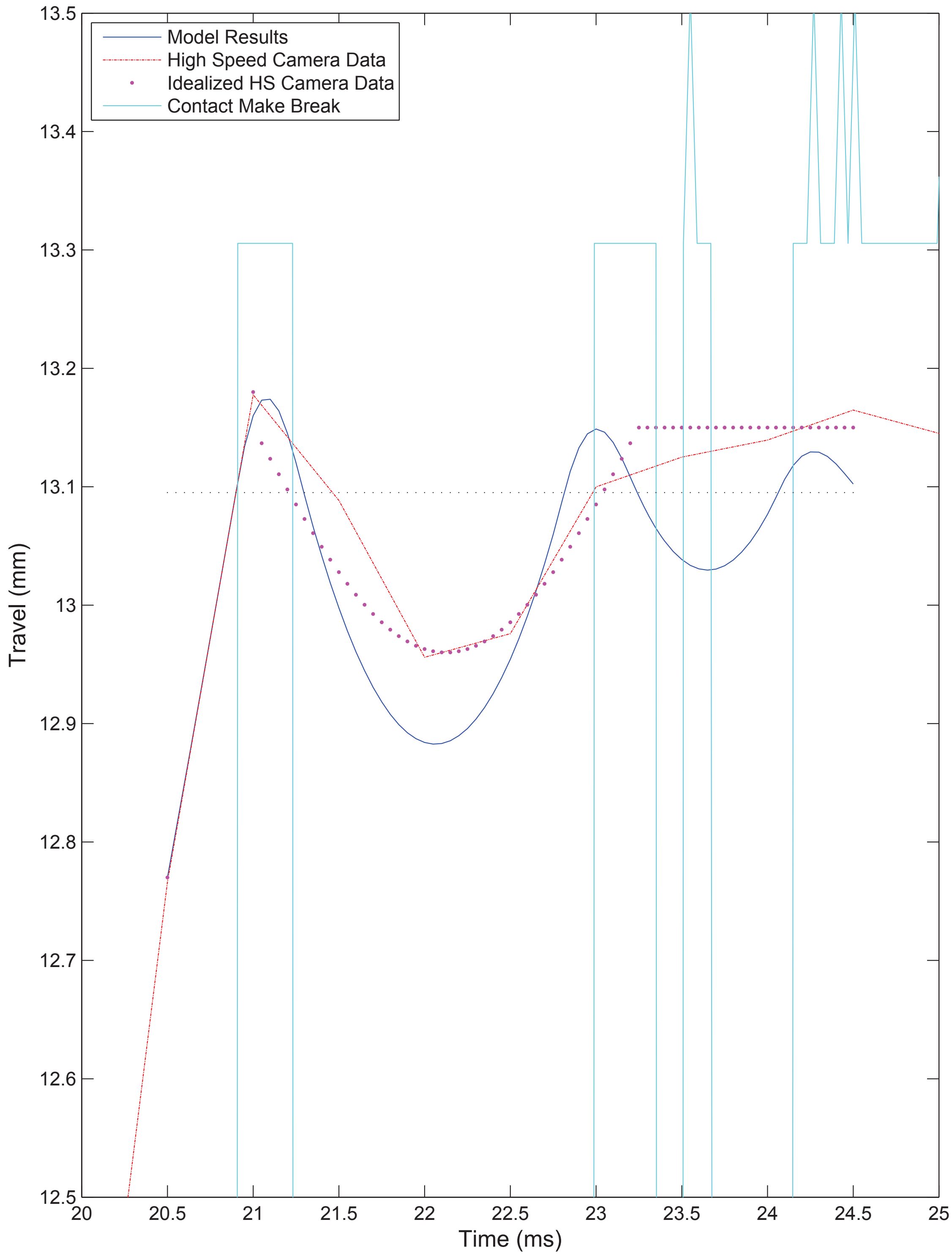

Figure 4.14: Contact bounce model (using optimized spring/damper values of $k_{fc} \approx 4.5 \times 10^7 N/m$ and $c_{fc} \approx 3.7 \times 10^3 Ns/m$) shown with the high speed camera data and make-break test results.

approximately 2.12 g and 2.67×10^{-7} m^3 of copper. Therefore, it would require 19.46 J of energy to break this (ideal) weld (using Eqn. 2.14). From this value, Eqn. 2.14 can be rearranged to calculate the value of the α term, as shown below.

$$\alpha = \frac{E_{BW}}{E_{TH}} = \frac{2.15J}{19.46J} = 0.11 \tag{4.4}$$

This factor can be applied to subsequent welds to account for the imperfections, stress concentrations, and any leveraging effects of an imperfect system. For example, using this factor to scale the forces seen in the worst-case-scenario actual weld-break yields the force vs extension curve shown in Fig. 4.15. There is much additional testing that must be done in order to develop a weld-strength model with higher fidelity. However, this is a time and capital intensive exercise. Regardless, the weld-strength model is a key model that is needed for the proper sizing of the magnetic actuator. Improvements to this model will be discussed further in the examination of the future work.

4.3.1 Alternate Model Variations

The purpose of this subsection is to briefly discuss an alternative weld-strength model variations that was examined. It is based on the fact that the interrupter uses AMF contacts, which result in a diffuse arc that covers the entire surface of the contact. Therefore, the assumption that a localized weld will be formed might not be accurate. There is also a counterbore in the center of the contact, preventing welding directly in the middle of the contact. This counterbore helps reduce the area of the contact that can actually be welded and ensures that the leveraging effects of offset welds can be utilized. Therefore, there is a certain area that is brought into contact when the fixed contact and the free contact meet, which can be called the weldable region. As is used in the above weld-strength model, the amount of melted copper can be determined from the amount of energy input to the contacts during arcing. Therefore the volume of melted material is known and the contact area is known, so the depth of melted material can be calculated. Now the area and length of the weld is known, so Johnson's stress strain curve [1] can be used to calculate the forces needed to break this weld. However,

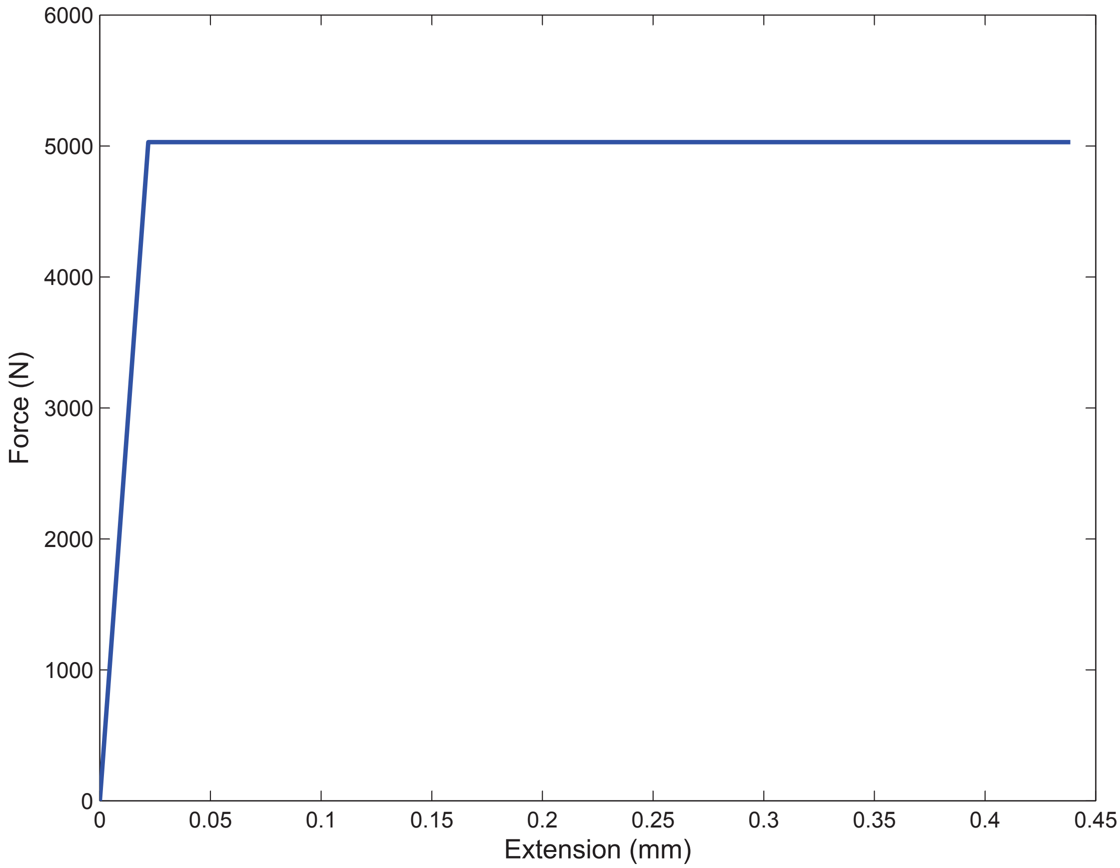

Figure 4.15: Adjusted force vs extension plot predicted for a more realistic weld.

using this method, the force required to break the weld is much higher than the current parts are designed for. This fact leads one to believe that one of the assumptions inherent in this model are incorrect. The proposed tests described in Section 6.2 will help determine an improved model.

4.4 Summary

This chapter presented the methods and results of the determination of several parameters used as submodels within the overall dynamic model. It was found that dielectric breakdown and recovery can be modeled as occurring at the first peak voltage level after some critical gap value. Additionally, the constants required for the contact model and the weld-strength model were determined. Now that the model is complete, the following chapter will compare the performance of the system with experimental data to determine the validity of the model.

CHAPTER 5

Model Verification

In order to ensure that the model is providing reasonable results, it is imperative that the simulation results be compared to experimental data. In this case, the comparison will be based on the travel traces that describe the motion of the unattached mass. Because high-voltage testing requires the attached mass to be energized and any attempt to cut a hole in the epoxy encapsulation would result in a loss of electrical insulation, the attached mass travel trace is not available. Therefore, the unattached mass travel will be used as an assessment of the total system motion. Additional verification will come from a comparison of the contact bounce time.

5.1 Travel Trace Comparison

The model parameters determined in Chapters 2 and 4 were implemented in the dynamic model and the simulation was run. The resulting data was plotted and overlayed with the experimental data, as shown in Fig. 5.1. Overall, good agreement is seen. The opening operation simulation matches the experimental data extremely well. The slight discrepancy at the end of the opening travel is probably due to the fact that the simulation does not account for the dynamics of the unattached mass once it has reached its stroke length. This assumption prevents the oscillations seen at the end of the opening travel.

There are several differences between the simulated and experimental data during the closing operation. The first and most obvious is that general divergence of the simulated data from the experimental data as the position values increase. This discrepancy is most likely due to the fact that the actuator was modeled as providing a constant force value. As the actuator is a complicated system of permanent magnets and a powerful coil, it is reasonable that there would be some change in the force. In this case, it appears that the force is decreasing.

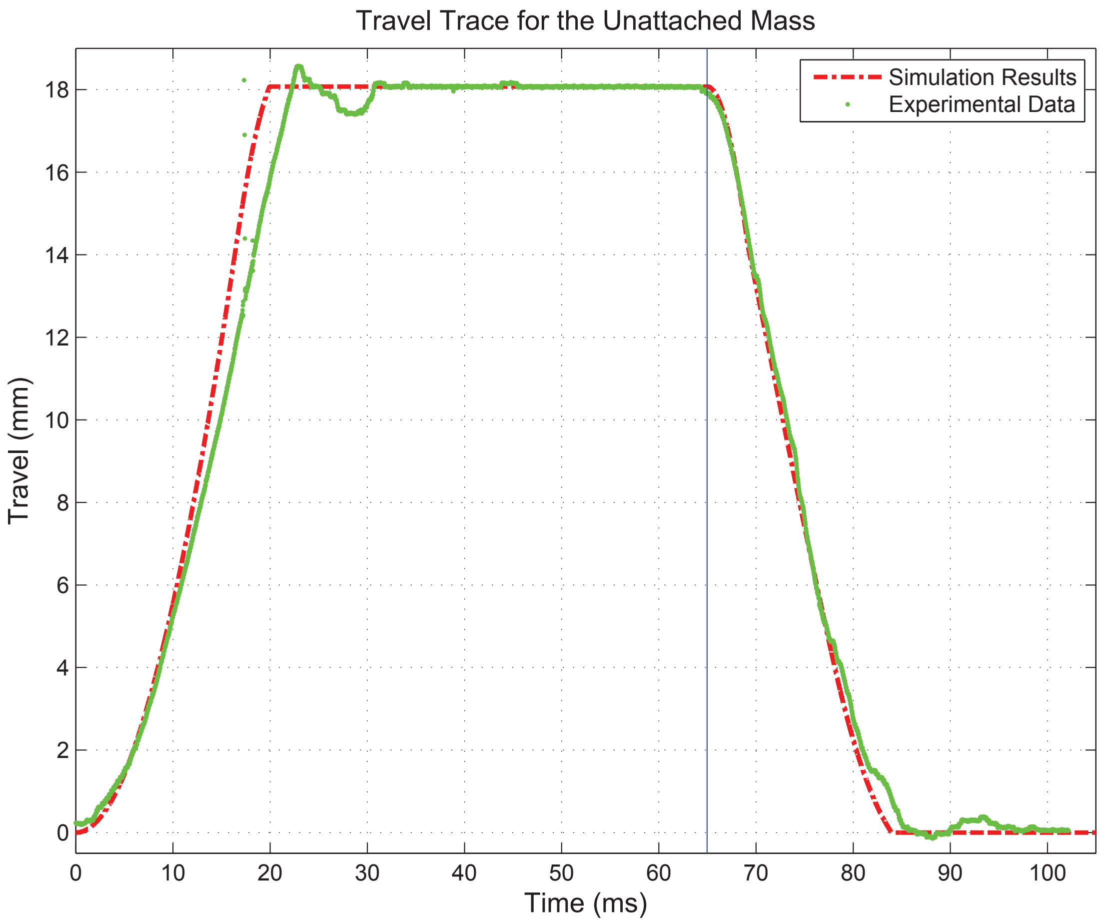

Figure 5.1: Comparison of the simulated system response with experimental data.

Figure 5.1 also shows considerable oscillation in the experimental data at the end of the closing stroke (at approximately 20-30 ms). This oscillation in the data is probably not due to actual oscillations of the unattached mass. The experimental data was recorded using a resistive position indicator. This tool has an eye-socket that a pylon rests in and drags the resistance-changing shaft to track the motion of the unattached mass. Due to the high speeds and sudden stop at the end of the closing stroke, it is possible that the pylon supporting the eye-socket is experiencing some cantilever-style vibrations.

5.2 Contact Bounce Time Comparison

The motion of the attached mass must also be verified. This verification can be done using the experimental contact make-break tests used in Section 4.2. The simulated travel trace for the attached mass (m_1) is shown below in Fig. 5.2. The

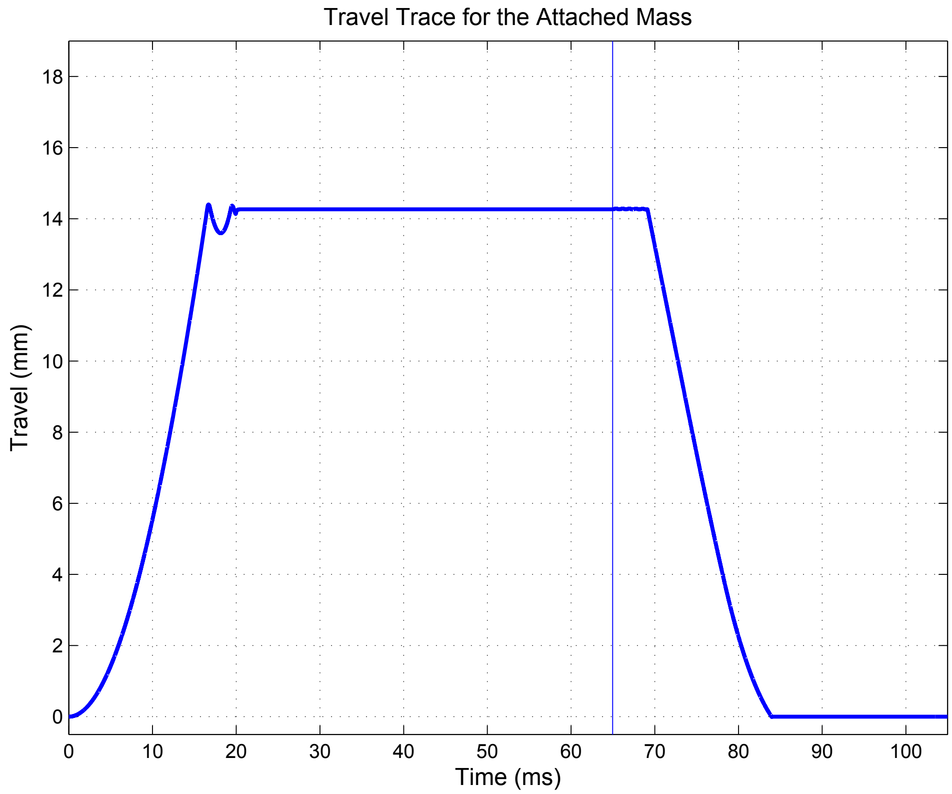

Figure 5.2: Simulated travel trace for the attached mass.

main factor of interest on the attached mass travel trace is the amount of time spent arcing during the contact bounce. In order to measure this, a comparison will be made between the amount of time spent with the contacts separated after initial impact and the amount of time the make-break tests show separation. The make-break tests show approximately 2.4 ms of time of contact bounce. Figure 5.3 shows the simulated travel trace for the attached mass with the contact separation times noted. This simulation shows a total of 2.755 ms of contact bounce, approximately a 13% difference. These values are reasonably close, lending credence to the model for the motion of the attached mass.

5.3 Discussion

The two above sections present two different methods of measuring the validity of the model relative to experimental data. The travel trace comparison showed reasonable agreement, with some modeling assumptions causing a slight

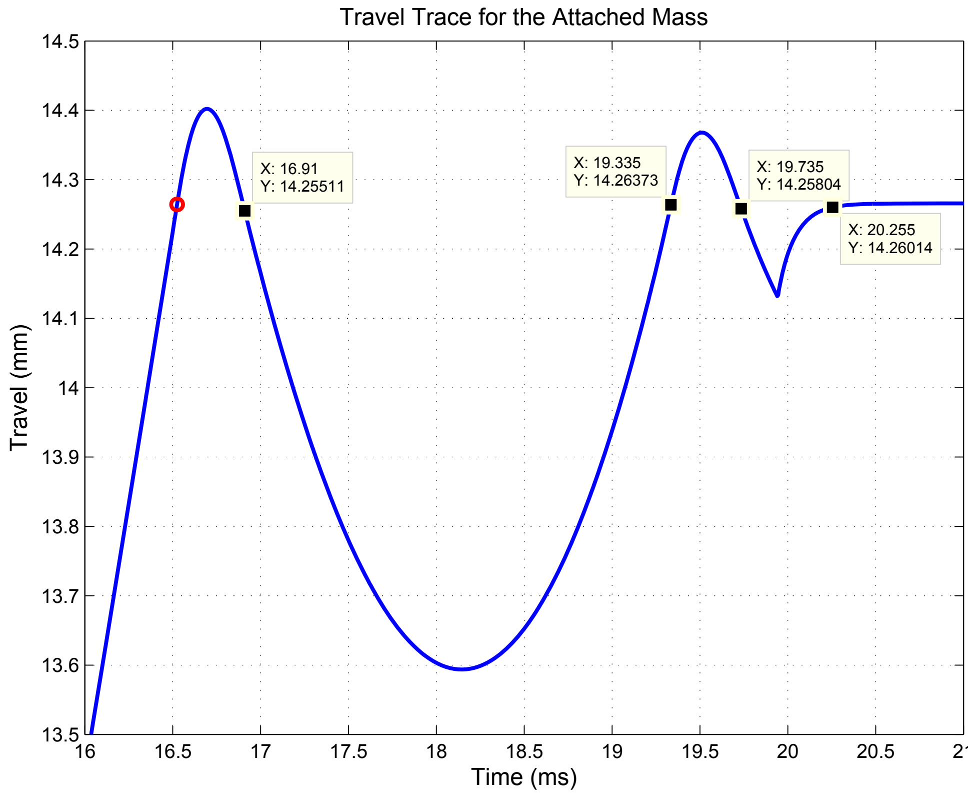

Figure 5.3: Simulated travel trace for the attached mass with the contact separation times called out.

difference between the simulation and the experimental data for the closing operation. The contact bounce comparison shows a difference of 13%. This value is fairly small, given the simplicity of the model used to represent the contact between the fixed contact and the attached mass. Greater agreement could be achieved which a contact model that featured additional tuning parameters (which will be discussed in the next section). Based on these two metrics, it can be said that the model is reasonably accurate.

CHAPTER 6

Conclusions

The design of automatic circuit reclosers is generally done based on rules of thumb and iterative methods. This approach produces systems that are able to operate with great longevity, but often results in systems that are overpowered and inefficient. The purpose of this thesis is to develop a dynamic model of an automatic circuit recloser to assist in the design process. This dynamic model was successfully created along with several additional contributions, as outlined in the next section.

6.1 Contributions of this Research

The contributions of this research are as follows:

- A dynamic model of an automatic circuit recloser was created and verified. The combination of models here cannot be overlooked; this thesis provides a single source of information with considerable background and discussion of application of a number of sub-models used within the overall dynamic model.
- A new model for dielectric breakdown was established based on the voltage level, rather than the widely used electric field method.
- A contact bounce model was established that is able to match the experimental data on a time basis.
- A weld model that accounts for weld imperfections was established.
- An energy analysis demonstrating the trivial nature of characteristics of the contact pressure spring for reasons other than the maintenance of a high constriction area.

The last item involved the emphasis that the only energy available to break the weld was that which was supplied by the actuator. This simplified energy perspective can be used to calculate a rough actuator force required. The greater detail of the dynamic model can be used to fine-tune the system, using the calculated values as a starting point. However, the model requires higher fidelity before being truly useful for this purpose. To this end, the following paragraphs will be an examination of the future work that must be conducted to increase the fidelity of this model.

6.2 Future Work

There are several individual models that could be improved within the dynamic model, but none are as important as the weld-strength model. This model is both the most important and the most complicated of the models. Further research should be carried out to determine better methods for determining:

- weld size
- weld location
- weld strength
- weld behavior at high strain rates
- effect of contact composition

It is the author's opinion that this could best be carried out by molding several vacuum interrupters and performing a series of high-voltage operations at varying current and voltage levels and for a varying number of operations. The voltage and current values should be preserved along with the travel values for the purpose of estimating the amount of energy that was absorbed by the contacts during the arcing process. The vacuum interrupters could then be removed from their encapsulation (while preserving their welds) and placed in a high-strain rate tensile testing machine that would produce speeds similar to those seen during the opening process. High speed camera and force vs extension data should be recorded for the purpose of estimating the amount of energy absorbed during the weld-break and the mode of fracture (ductile/brittle). This process will be a capital and time intensive exercise, but will allow for the direct characterization and description of the welds that will need to be broken by the ACR's mechanism. This data will ultimately allow for the determination of the actuator that can provide the ideal amount of energy.

The fidelity of the contact bounce model could also be improved. The present model produces roughly accurate times for total bouncing, but the travel of the attached mass differs considerably. This difference is most likely due to the relatively simple Kelvin-Voight model used. Coefficient of restitution methods lack the time dependence that must be modeled if the contact motion is to be used to determine the weld strength (e.g., He et al. [16] used a coefficient of restitution approach, but showed prolonged bouncing not seen in the experimental data). In order to properly model the motion seen in the experimental data, a new model must be created with additional parameters. The addition of the stiffness of the support structure could also be considered as in [17]. These parameters would allow the optimization routine to search a larger area, resulting in a closer match between the model and experimental data. The development of this contact bounce model would help improve the overall fidelity of the dynamic model.

Other avenues for further development include a greater understanding of the events occurring during dielectric breakdown. The work presented in this thesis stopped once a model with acceptable fidelity was developed, but there are still many more questions to be answered. The most intriguing is how the constant voltage model used in this model can be reconciled with the historically used enhanced electric field model. Further test data should be analyzed to determine the effects due to different styles of vacuum interrupter, contact composition, contact surface finish, and contact shape. Historically, these should all play a part in the breakdown process. However, if breakdown always occurs at a peak voltage level, then there is no need for the intense contact surface processing that is currently used (or at least a reduced amount of processing).

Another region for great model improvement lies in the actuator model. Now that it is truly understood how important the output of the actuator is, a proper model of the actuator must be created. This actuator model would assist in the design of the actuator and the prediction of its behavior within the ACR. Finally, in order for the model to accurately capture the weld-breaking process, the interface between the pin and the end of the slot in the lost motion mechanism must be better understood. Any energy lost to elastic/plastic deformation of the slot or pin is energy that cannot be used to break the weld. Therefore, the modeling and improvement of this feature is essential.

6.3 Final Conclusion

The dynamic model of an automatic circuit recloser presented in this thesis provides a blueprint for the further development and optimization of the weld-breaking motion. This model is useful for the determination of the motion of the attached and unattached mass given the system parameters as an input. While model is not perfect, it helps expose the knowledge gaps and the models that require improvement. The above paragraphs indicate several of these models and outlines tests that can be done to provide the additional data needed to achieve a model with the fidelity required to truly determine the optimal weld-breaking mechanism.

APPENDIX A

Dynamic Model Simulation Code

The following sections provide the simulation code for the dynamic model.

A.1 Master File

```
clear all
close all
clc
format compact

global xclosing tclose_start tclose_stop topen_start topen_stop do...
    ot V I freq m1 m2 wframp kcp lo li kb Fbo vioffset ks cs kfc cfc...
    ks2 cs2 g E_hardness Fotemp Fctemp Fh rcontact Acontact stroke...
    DryFriction

%% Initializations
V = 30500; % Volts
I = 17.67*1000; % Amps
freq = 60; % Hertz

tclose_start = 0; % sec
tclose_stop = .04; % sec
topen_start = tclose_start + 0.06497; % sec
topen_stop = topen_start+0.04; % sec

vioffset = -0.01067; % s

Fctemp = 100; % N
Fotemp = Fctemp; % N
Fh = 0; % N
DryFriction = 0; % N

do = 14.26; % mm
do = do/1000; % m
ot = 3.81; % mm
ot = ot/1000; % m
stroke = do+ot; % m

kcp = 58.3; % N/mm
kcp = kcp*1000; % N/m
kcp = kcp; % N/m
lo = 49; % mm
lo = lo/1000; % m
li = 42.16; % mm 42.16
li = li/1000; % m

m1 = 0.7239; % kg
m2 = 1.61; % kg
g = 9.807; % m/s^2

kb = 99.471; % N/cm
kb = kb*100; % N/m
Fbo = 49.451; % N

ks = 10^10; %N/m  Stiffness of spring used to model contact at stopper
cs = 10^6; %Ns/m Damping of damper used to model contact at stopper
```

```
ks2 = ks; % 1000000; % N/m
cs2 = cs; % 100000; % Ns/m

kfc = 4.5*10^7; % N/m contact/contact spring
cfc = 3.7*10^3; % Ns/m contact/contact damper
%     kfc = (8.7812*10^11)*10^4;
%     cfc = (1.4781*10^12)*10^4;

E_copper = 3*10^8; % N/m^2 From Martin Leusenkamp email
E_hardness = 35*9.8*10^6; % N/m^2

rcontact = 1.75/2; % in
rcontact = rcontact*0.0254; % m
Acontact = pi*rcontact^2; % m^2

FinderClose = [];
FinderOpen = [];
arcresults = zeros(6,1);
permanentarcstart = 0;
permanentarcstop = 0;
programstoptime = 0;
ContactCompressionForce = 0;

%% Run the Closing Solver

ClosingMechSolver_Electric
xclosing = x;
tspan_closing = tspan;
x = [];
tspan = [];

%% Run the Intermediate Solver
x0_int = [xclosing(end,1) xclosing(end,2) xclosing(end,3) ...
    xclosing(end,4) xclosing(end,5) xclosing(end,6) xclosing(end,7)...
    xclosing(end,8)];
[tspan_int x_int] = ode45('IntMech',...
    [tclose_stop:.000005:topen_start],x0_int);

%% Check for When Arcing Happens
x_ac = [xclosing; x_int];
tspan_ac = [tspan_closing; tspan_int];
tas0 = []; xas0 = []; gapas0 = [];
tasf = []; xasf = []; gapasf = [];
arccheck = 0; hitcheck = 0;

for iac = 1:length(x_ac)
    gapac(iac) = (do*1000)-(x_ac(iac,1)*1000); % mm
    voltageac(iac) = x_ac(iac,5)/1000; % Volts
    EoB(iac) = voltageac(iac)/gapac(iac); % Volts/mm

    if gapac(iac)<=0
        hitcheck = 1;
    end
    if ((gapac(iac)>0)&&(ArcStart(gapac(iac)/1000,x_ac(iac,5))==1)...
            &&(arccheck==0))||((hitcheck==1)&&(arccheck==0)...
            &&(gapac(iac)>0))
        tas0 = [tas0 tspan_ac(iac)]; % sec
        xas0 = [xas0 x_ac(iac)]; % m
        gapas0 = [gapas0 gapac(iac)]; % mm
        arccheck = 1;
    end
    if ((gapac(iac)<=0)&&(arccheck==1))
        tasf = [tasf tspan_ac(iac)]; % sec
        xasf = [xasf x_ac(iac)]; % m
        gapasf = [gapasf gapac(iac)]; % mm
        arccheck = 0;
    end
end
```

```
x= [xclosing; x_int];
tspan = [tspan_closing; tspan_int];

%% Determine Weld Characteristics
numbarcs = length(tasf);
for i = 1:numbarcs
    arcenergy(i) = ...
        abs(ArcVoltage2(tas0(i),I)*((-I*cos(2*pi*freq*(vioffset+tasf(i)))...
        +I*cos(2*pi*freq*(vioffset+tas0(i))))/(2*pi*freq)));
    % without the absolute values
    for iw = 1:100
        timesteps = linspace(tas0(i),tasf(i),100);
        ArcV = ArcVoltage2(timesteps(iw),I);
        [closestt closesti] = min(abs(tspan-timesteps(iw)));
        Current = x(closesti,7);
        energyin(iw) = abs(ArcV*Current)*((tasf(i)-tas0(i))/100);
    end
    arcenergy2(i) = sum(energyin);
    energyin = [];
end
totalarcenergy = sum(arcenergy);
totalarcenergy2 = sum(arcenergy2);

% Determine the actual contact area
contactforce = kfc*(xclosing(end,1)-do); % N
constrictionarea = contactforce/E_hardness; % m^2
constrictionradius = sqrt(constrictionarea/pi); % m constriction
% radius without blow off forces

arearatio = constrictionarea/Acontact; % m^2/m^2 tells us how much of
% the contacts are touching

totalarcenergy = totalarcenergy2; % J
cv = 0.385; % J/g-C specific heat of copper
Tm = 1083.4; % C melting temperature of copper
T0 = 20; % C initial temperature of copper
cL = 204.8; % J/g
copperdensity = 7.94*10^6; % g/m^3
meltedmass = totalarcenergy/(cv*(Tm-T0)+cL); % grams, mass of resultant weld
meltedvolume = meltedmass/copperdensity; % m^3, volume of weld
weldvolume = meltedvolume;
weldradius = ((meltedvolume*3)/(4*pi))^(1/3); % m
weldarea = pi*weldradius^2; % m^2
Fwmax = 127*(totalarcenergy^(2/3)); % N, weld force
FractureEnergyperV = 72.99*10^6; % J/m^3 fracture energy of pure annealed copper
ETH = FractureEnergyperV*meltedvolume; % J theoretical energy needed to break weld
alpha = 0.11; % calculated adjustment factor
EBW = ETH*alpha; % J actual energy needed to break weld
maxweldextension = EBW/(.975*Fwmax); % m
maxweldextensionalpha = maxweldextension*(alpha^(1/2));
Fwmaxalpha = Fwmax*(alpha^(1/2));

%% Run the Opening Solver
arcresults = ones(6,1);
OpeningMechSolver_Electric
xopening = x;
xopening(:,1) = do-xopening(:,1);
xopening(:,3) = (do+ot)-xopening(:,3);
tspan_opening = tspan;
x = [];
tspan = [];

x = [xclosing; x_int; xopening];
tspan = [tspan_closing; tspan_int; tspan_opening];
```

A.2 Closing Operation Solver

```
%% Initial Conditions and Time Stepping
global V I vioffset tclose_start tclose_stop freq
```

```
x01 = 0; % m
xdot01 = 0; % m/s
x02 = 0; % m
xdot02 = 0; % m/s
V0 = V*sin(2*pi*freq*(vioffset+tclose_start)); % Volts, initial
                                                % condition of voltage
Vdot0 = V*freq*2*pi*cos(2*pi*freq*(vioffset+tclose_start)); % Volts/s,
                              % initial condition of derivative of voltage
I0 = I*sin(2*pi*freq*(vioffset+tclose_start)); % Amps, initial
                                                % condition of current
Idot0 = I*freq*2*pi*cos(2*pi*freq*(vioffset+tclose_start)); % Amps/s,
                               % initial condition of derivative of current
x0 = [x01 xdot01 x02 xdot02 V0 Vdot0 I0 Idot0]; % 0 0]; % initial conditions
hitcheck = 0;

tstart = tclose_start; % sec
tstop = tclose_stop;

tarc = []; % arcing time empty vector
arcingstartcheck= 0;
tas0 = [];
xas0 = [];
tastop = [];

%% Run the solver
[tspan,x] = ode45('ClosingMech_Electric',[tstart:0.000005:tstop],x0);
```

A.3 Closing Operation Function

```
function [xout] = ClosingMech_Electric(t,x0)

global V I cfc kfc ks cs ks2 cs2 vioffset do ot freq m1 m2 kcp lo li...
    kb Fbo g Fctemp Fh Acontact rcontact E_hardness DryFriction stroke


Fc = Fctemp;
% Initializations
stroke = stroke; % m
arcstartfactor = .7; % obtained from E/Beta plots by looking at
                     % when the earliest arcs are started
tstep = 0.00001; %sec

%% Current and Voltage Diff Eqs
Vdot(1) = x0(6);
Vdot(2) = -V*freq*freq*4*pi^2*sin(2*freq*pi.*(t+vioffset));

Idot(1) = x0(8);
Idot(2) = -I*freq*freq*4*pi^2*sin(2*freq*pi.*(t+vioffset));


%% Determine When Arcing Starts
if (evalin('base','permanentarcstart')==0)
    if (ArcStart(do-x0(1),x0(5))==1)
        arcresultstemp = 1;
    else
        arcresultstemp = 0;
    end
    if abs(do-x0(1))<0.0005
        arcresultstemp = 1;
    end
    if abs(do-x0(1))>0.003
        arcresultstemp = 0;
    end

    assignin('base','arcresults',[evalin('base','arcresults'); arcresultstemp]);

    if (mean(evalin('base','arcresults(end-5:end)'))>0.5)...
            &&(evalin('base','permanentarcstart')==0)
```

```
        assignin('base','permanentarcstart',1);
        assignin('base','programarcstarttime',t);
    end
end


%% Attractive Magnetic Force
if evalin('base','permanentarcstart')==1
    F_magattract = AttractiveMagneticForce((do-x0(1)),I); % magnetic
                                                        % attractive forces
else
    F_magattract = 0;
end

%% Blow Off Force
if (x0(1)>=do)
    constrictionarea = abs((kfc*(x0(1)-do)+cfc*abs(x0(2))))/E_hardness; % m^2
    constrictionradius = sqrt(constrictionarea/pi); % m
    if constrictionradius>rcontact
        constrictionradius = rcontact;
    end
    F_mbo = (10^-7)*x0(7)^2*log(rcontact/constrictionradius); % N,
                                                % magnetic blow off forces
else
    F_mbo = 0;
end

%% Adding Up The Electrical Forces
if (evalin('base','permanentarcstart')==1)&&(x0(1)<(do))
    F_electric = F_magattract; % N, just attractive magnetic forces here
elseif (evalin('base','permanentarcstart')==1)&&(x0(1)>=do)
    F_electric = -F_mbo+F_magattract; % N, add blow off forces here
else
    F_electric = 0;
end

%% Calculate the Damping Value for This Step
if x0(2)>0;
     cfcnonlin = cfc;
else
    cfcnonlin = 0;
end

%% State Space

if (x0(1)<do)&&(x0(3)<stroke)&&((x0(3)-x0(1))<=0) % APPROACH PHASE %%%%%%%
    zdot(1) = x0(2);
    zdot(2) = (1/m1)*(kcp*(lo-li-x0(1)+x0(3))+Fbo+kb*(do-x0(1))-m1*g...
        +F_electric+ks*(x0(3)-x0(1))+cs*(x0(4)-x0(2)));

    ydot(1) = x0(4);
    ydot(2) = (1/m2)*(Fc-kcp*(lo-li-x0(1)+x0(3))-m2*g-ks*(x0(3)-x0(1))...
        -cs*(x0(4)-x0(2))-DryFriction*sign(x0(4)));

elseif (x0(1)<do)&&(x0(3)<stroke)&&((x0(3)-x0(1))>0)
    zdot(1) = x0(2);
    zdot(2) = (1/m1)*(kcp*(lo-li-x0(1)+x0(3))+Fbo+kb*(do-x0(1))-m1*g...
        +F_electric);

    ydot(1) = x0(4);
    ydot(2) = (1/m2)*(Fc-kcp*(lo-li-x0(1)+x0(3))-m2*g...
        -DryFriction*sign(x0(4)));

elseif (x0(1)>=(do))&&(x0(3)<(stroke)) % COMPRESSION PHASE %%%%%%%%%%%%%

    if ((x0(3)-x0(1))<=0)
        zdot(1) = x0(2);
        zdot(2) = (1/m1)*(kcp*(lo-li-x0(1)+x0(3))+Fbo+kb*(do-x0(1))-m1*g...
            +F_electric+ks*(x0(3)-x0(1))+cs*(x0(4)-x0(2))-kfc*(x0(1)-do)...
```

```
            -cfcnonlin*x0(2));

        ydot(1) = x0(4);
        ydot(2) = (1/m2)*(Fc-kcp*(lo-li-x0(1)+x0(3))-m2*g...
            -DryFriction*sign(x0(4)));

    elseif ((x0(3)-x0(1))>0)
        zdot(1) = x0(2);
        zdot(2) = (1/m1)*(kcp*(lo-li-x0(1)+x0(3))+Fbo+kb*(do-x0(1))...
            -m1*g+F_electric-kfc*(x0(1)-do)-cfcnonlin*x0(2));

        ydot(1) = x0(4);
        ydot(2) = (1/m2)*(Fc-kcp*(lo-li-x0(1)+x0(3))-m2*g...
            -DryFriction*sign(x0(4)));
    end

elseif (x0(1)>=do)&&(x0(3)>=(stroke)) % TERMINAL PHASE %%%%%%%%%%%%%%%%%%%

    zdot(1) = x0(2);
    zdot(2) = (1/m1)*(kcp*(lo-li-x0(1)+x0(3))+Fbo+kb*(do-x0(1))-m1*g...
        +F_electric-kfc*(x0(1)-do)-cfcnonlin*x0(2)+ks2*(x0(3)-ot-x0(1))...
        +cs2*(x0(4)-x0(2)));

    ydot(1) = x0(4);
    ydot(2) = -(x0(4)/tstep);

elseif (x0(1)<(do))&&(x0(3)>=(stroke)) % CHATTER PHASE %%%%%%%%%%%%%%%%%%%
    zdot(1) = x0(2);
    zdot(2) = (1/m1)*(kcp*(lo-li-x0(1)+x0(3))+Fbo+kb*(do-x0(1))-m1*g...
        +F_electric+ks2*(x0(3)-ot-x0(1))+cs2*(x0(4)-x0(2)));

   ydot(1) = x0(4);
   ydot(2) = -(x0(4)/tstep);
else
    ydot(1) = 0;
    ydot(2) = 0;
    zdot(1) = 0;
    zdot(2) = 0;
end

xout(1) = zdot(1);
xout(2) = zdot(2);
xout(3) = ydot(1);
xout(4) = ydot(2);
xout(5) = Vdot(1);
xout(6) = Vdot(2);
xout(7) = Idot(1);
xout(8) = Idot(2);

xout = xout';
end
```

A.4 Opening Operation Solver

```
global V I topen_start topen_stop do ot xclosing vioffset freq

%% Initial Conditions

x01 = do-xclosing(end,1);
xdot01 = 0;
x02 = (do+ot)-xclosing(end,3);
xdot02 = 0;
V0 = V*sin(2*pi*freq*(vioffset+topen_start)); % Volts, initial
                                                     % condition of voltage
Vdot0 = V*freq*2*pi*cos(2*pi*freq*(vioffset+topen_start)); % Volts/s,
                               % initial condition of derivative of voltage
I0 = I*sin(2*pi*freq*(vioffset+topen_start)); % Amps, initial condition
                                                             % of current
Idot0 = I*freq*2*pi*cos(2*pi*freq*(vioffset+topen_start)); % Amps/s,
```

```
                                % initial condition of derivative of current
x0 = [x01 xdot01 x02 xdot02 V0 Vdot0 I0 Idot0]; % initial conditions
tstart = topen_start;
tstop = topen_stop;

%% Run the solver
[tspan, x] = ode45('OpeningMech_Electric',[tstart:0.000005:tstop],x0);
```

A.5 Opening Operation Function

```
function [xout] = OpeningMech_Electric(t,x0)

global V I cfc kfc ks cs vioffset freq do ot m1 m2 kcp lo li Fbo kb...
    g Fotemp rcontact stroke DryFriction

% Initializations
tstep = 0.00001;

Fo = Fotemp-(Fotemp)*(x0(3)/stroke);

%% Current and Voltage Diff Eqs
Vdot(1) = x0(6);
Vdot(2) = -V*freq*freq*4*pi^2*sin(2*freq*pi*(t+vioffset));

Idot(1) = x0(8);
Idot(2) = -I*freq*freq*4*pi^2*sin(2*freq*pi*(t+vioffset));


%% Determine When Arcing Stops
if (evalin('base','permanentarcstop')==0)
    if (ArcStop(x0(1),x0(5))==1)
        arcresultstemp = 0;
    else
        arcresultstemp = 1;
    end
    if x0(1)<0.002
        arcresultstemp = 1;
    end
    if x0(1)> 0.009
        arcresultstemp = 0;
    end

    assignin('base','arcresults',[evalin('base','arcresults'); arcresultstemp]);

    if (mean(evalin('base','arcresults(end-5:end)'))<0.5)...
            &&(evalin('base','permanentarcstop')==0)
        assignin('base','permanentarcstop',1);
        assignin('base','programarcstoptime',t);
    end
end


%% Attractive Magnetic Force
if evalin('base','permanentarcstop')==0
    F_magattract = AttractiveMagneticForce(x0(1),I); % magnetic attractive forces
else
    F_magattract = 0;
end

%% Blow Off Force
if (x0(1)<=evalin('base','maxweldextension'))
    if (x0(1)<=0)
        constrictionarea = evalin('base','weldarea');
        constrictionradius = sqrt(constrictionarea/pi);
    elseif (x0(1)>0)&&(x0(1)<evalin('base','maxweldextension'))
        % for magnetic blow off forces, assume constant volume cylinder, so as
        % length increases, the constriction radius decreases
        constrictionareatemp = ...
            evalin('base','weldvolume')/(evalin('base','weldradius')+x0(1));
```

```
        constrictionradiustemp = sqrt(constrictionareatemp/pi);
        constrictionradius = constrictionradiustemp;
    end
    if ((x0(1)<=0)&&((kfc*(x0(1))+cfc*(abs(x0(2))))>0))||...
            ((x0(1)>0)&&(x0(1)<evalin('base','maxweldextension')))
        F_mbo = (10^(-7))*(x0(7)^2)*log(rcontact/constrictionradius); % N,
                                                  % magnetic blow off forces
    else
        F_mbo = 0;
    end
else
    F_mbo = 0;
end

%% Weld Force
Fw = FwFinal(do-x0(1),evalin('base','maxweldextensionalpha'),...
    evalin('base','Fwmaxalpha'));

%% Adding Up The Electrical Forces
if x0(1)<0
    F_electric = -F_magattract+F_mbo; % N
elseif (x0(1)<=evalin('base','maxweldextension'))&&(x0(1)>0)
    F_electric = -Fw-F_magattract+F_mbo; % N
elseif (evalin('base','permanentarcstop')==0)...
        &&(x0(1)>evalin('base','maxweldextension'))
    F_electric = -F_magattract; % N
else
    F_electric = 0;
end

%% Calculating the Nonlinear Damping Coefficient
cfcnonlin = cfc*abs(x0(1));
if x0(3)< do;
    cstop = 0;
else x0(3) > do;
    cstop = 200; %Ns/m
end

%% Mechanical Interactions

if x0(3)<ot % EXTENSION PHASE %%%%%%%%%%%%%%%%%%%%%%%%%%%%%%%%%%%%%%%%%%%%%%%
    zdot(1) = x0(2);
    zdot(2) = (1/m1)*(-kcp*(lo-li+ot+x0(1)-x0(3))-Fbo-kb*(x0(1))...
        +m1*g+kfc*(-x0(1))+F_electric);

    ydot(1) = x0(4);
    ydot(2) = (1/m2)*(Fo+kcp*(lo-li+ot+x0(1)-x0(3))+m2*g...
        -DryFriction*sign(x0(4)));

elseif (x0(3)>=ot)&&(x0(3)<stroke) % RETREAT PHASE %%%%%%%%%%%%%%%%%%%%%%
    zdot(1) = x0(2);
    zdot(2) = (1/m1)*(-kcp*(lo-li+ot+x0(1)-x0(3))-Fbo-kb*(x0(1))...
        +m1*g+ks*(x0(3)-ot-x0(1))+cs*(x0(4)-x0(2))+F_electric);

    ydot(1) = x0(4);
    ydot(2) = (1/m2)*(Fo+kcp*(lo-li+ot+x0(1)-x0(3))+m2*g...
        -ks*(x0(3)-ot-x0(1))-cs*(x0(4)-x0(2))-DryFriction*sign(x0(4))...
        -cstop*x0(4));

elseif x0(3)>=stroke % STOP UNATTACHED MASS %
    zdot(1) = x0(2);
    zdot(2) = (1/m1)*(-kcp*(lo-li+ot+x0(1)-x0(3))+m1*g-Fbo-kb*x0(1)...
        +ks*(x0(3)-ot-x0(1))+cs*(x0(4)-x0(2))+F_electric);

    ydot(1) = 0;
    ydot(2) = -(x0(4)/tstep);
end

xout(1) = zdot(1);
```

```
xout(2) = zdot(2);
xout(3) = ydot(1);
xout(4) = ydot(2);
xout(5) = Vdot(1);
xout(6) = Vdot(2);
xout(7) = Idot(1);
xout(8) = Idot(2);

xout = xout';
end
```

A.6 Weld Force Function

```
function [ Fw ] = FwFinal(x0,maxweldextension,Fwmax)

force = [0 Fwmax Fwmax];
extension = [0 .05*maxweldextension maxweldextension];

if (x0<=evalin('base','maxweldextension'))
    Fw = interp1(extension,force,x0);
else
    Fw = 0;
end

end
```

A.7 Function for Determination of Dielectric Breakdown

```
function [ yesno ] = ArcStart(gap1,voltage)

gap = gap1*1000; % convert from m to mm
voltage = voltage/1000; % convert from V to kV

EoBeta = 30.595/gap; % kV/mm [for 38 kV]
% EoBeta = 21.072/(gap^0.959); % kV/mm [for 27 kV]

if gap <= .5
    yesno = 1;
end
if gap >= 3
    yesno =0;
end
if (gap>.5)&&(gap<3)
    if EoBeta > voltage/gap
        yesno = 0;
    elseif EoBeta <= voltage/gap
        yesno = 1;
    end
end
end
```

A.8 Function for Determination of Dielectric Recovery

```
function [ yesno ] = ArcStop(gap,voltage)

gap = gap*1000; % convert from m to mm
voltage = abs(voltage)/1000; % convert from V to kV

EoBeta = 30.978/(gap^0.989); % kV/mm [for 38 kV]
% EoBeta = 23.202/(gap^1.027); % kV/mm [for 27 kV]

if gap <= 2
    yesno = 0;
end
if gap >= 9
    yesno =1;
end
if (gap>2)&&(gap<9)
```

```
    if (EoBeta < voltage/gap)
        yesno = 0;
    elseif (EoBeta >= voltage/gap)
        yesno = 1;
    end
end

end
```

A.9 Function for Determination of Arc Voltage

```
function [ arcvoltage ] = ArcVoltage2(t,Ipk)

global vioffset

x = evalin('base','x');
tspan = evalin('base','tspan');
do = evalin('base','do')/1000;
[c index] = min(abs(tspan-t));
Irms = Ipk/sqrt(2);
Ii = Ipk*sin(2*pi*60*(vioffset+t));
arcvoltage = 46.96+(0.1528)*(Ipk/1000)*((do-x(index,1)))...
    -3.868*10+0.395*(Ii/1000)+(10^2)*0.139; %Volts
end
```

A.10 Function for Determination of the Attractive Magnetic Force Magnitude

```
function [ force ] = AttractiveMagneticForce(gap,Ipk)

% gap in meters
% current in Amps

if gap < 0
    gap = 0;
end

Irms = Ipk/sqrt(2);

current = (Irms)/1000; % convert from A to kA
force_temp = (-560.63*gap+32.8); % See excel sheet AttractiveForces.xls

% data collected for 12.5 kA --> correct by (newcurrent^2)/(12.5^2)

force = force_temp*((current^2)/(12.5^2));

end
```

REFERENCES

[1] G.R. Johnson and W.H. Cook. A constitutive model and data for metals subjected to large strains, high strain rates and high temperatures. In *Proceedings of the 7th International Symposium on Ballistics*, volume 21, pages 541–547. The Netherlands, 1983.

[2] P.G. Slade. *The Vacuum Interrupter: Theory, Design, and Application*. CRC Press, Boca Raton, Florida, US, 2008.

[3] S. Kulas. Welding when contacts close electrical circuits. *Electrical Contacts and Electrodes*, 2010.

[4] P.G. Slade. An investigation into the factors contributing to welding of contact electrodes in high vaccum. *Parts, Materials and Packaging, IEEE Transactions on*, 7(1):23–33, 1971.

[5] S.N. Kharin, H. Nouri, and T. Davies. The mathematical models of welding dynamics in closed and switching electrical contacts. In *Electrical Contacts, 2003. Proceedings of the Forty-Ninth IEEE Holm Conference on*, pages 107–123. IEEE, 2003.

[6] M. Kaplan and A. Tslaf. Criteria for the weldability of contact materials in adiabatic transient conditions. *Components, Hybrids, and Manufacturing Technology, IEEE Transactions on*, 7(1):33–38, 1984.

[7] Y. Kawase, H. Mori, and S. Ito. 3-D finite element analysis of electrodynamic repulsion forces in stationary electric contacts taking into account asymmetric shape. *Magnetics, IEEE Transactions on*, 33(2):1994–1999, 1997.

[8] W. Goldsmith. *Impact: The Theory and Physical Behaviour of Colliding Solids*. Edward Arnold Ltd., London, England, 1960.

[9] H.D. Bui. *Solid Mechanics and Its Applications: Fracture Mechanics*. Springer, P.O. Box 17, 3300 AA Dordrecht, The Netherlands, 2006.

[10] P.G. Slade and M.D. Nahemow. Initial separation of electrical contacts carrying high currents. *Journal of Applied Physics*, 42(9):3290–3297, 2003.

[11] A. Greenwood. *Vacuum switchgear*. Number 18. The Institution of Engineering and Technology, 1994.

[12] J. Newby (Editor). *ASM Metals Handbook, Vol. 8: Mechanical Testing (9th Ed.)*. ASM International, Materials Park, Ohio, US, 1989.

[13] MatWeb. Copper, cu; annealed.

[14] In *Private Communication*.

[15] In *Private Communication*.

[16] L. He, J.R. Mayor, R.G. Harley, H. Liles, G. Zhang, and Y. Deng. Multi-physics modeling of the dynamic response of a circuit breaker recloser system. In *Electric Machines & Drives Conference (IEMDC), 2013 IEEE International*, pages 1001–1008. IEEE, 2013.

[17] P. Barkan. A study of the contact bounce phenomenon. *Power Apparatus and Systems, IEEE Transactions on*, (2):231–240, 1967.